HHS Public Access

Author manuscript

*Phys Med Biol*. Author manuscript; available in PMC 2017 September 07.

Published in final edited form as:

*Phys Med Biol*. 2016 September 7; 61(17): R206–R248. doi:10.1088/0031-9155/61/17/R206.

# Image-guided ultrasound phased arrays are a disruptive technology for non-invasive therapy

**Kullervo Hynynen**[1,2,3] and **Ryan M. Jones**[1,2]

[1]Physical Sciences Platform, Sunnybrook Research Institute, Toronto, Canada

[2]Department of Medical Biophysics, University of Toronto, Toronto, Canada

[3]Institute of Biomaterials and Biomedical Engineering, University of Toronto, Toronto, Canada

## Abstract

Focused ultrasound offers a non-invasive way of depositing acoustic energy deep into the body, which can be harnessed for a broad spectrum of therapeutic purposes, including tissue ablation, the targeting of therapeutic agents, and stem cell delivery. Phased array transducers enable electronic control over the beam geometry and direction, and can be tailored to provide optimal energy deposition patterns for a given therapeutic application. Their use in combination with modern medical imaging for therapy guidance allows precise targeting, online monitoring, and post-treatment evaluation of the ultrasound-mediated bioeffects. In the past there have been some technical obstacles hindering the construction of large aperture, high-power, densely-populated phased arrays and, as a result, they have not been fully exploited for therapy delivery to date. However, recent research has made the construction of such arrays feasible, and it is expected that their continued development will both greatly improve the safety and efficacy of existing ultrasound therapies as well as enable treatments that are not currently possible with existing technology. This review will summarize the basic principles, current statures, and future potential of image-guided ultrasound phased arrays for therapy.

## 1. Introduction

During the past quarter century, there has been a realization that minimally-invasive interventions offer significant benefits to patients by reducing overall recovery times and lowering infection risks [1]. Indeed, these benefits could be even more dramatic if the interventions could be performed completely non-invasively.

The excellent penetration depth of ultrasound within soft tissues at millimeter-scale wavelengths provides an ideal method for non-invasive, localized energy delivery for tissue ablation and other interventions. Although the ability of focused ultrasound (FUS) to induce localized tissue coagulation was first demonstrated over 70 years ago [2, 3], its clinical adoption has been slow to date. The first clinical device utilized FUS beams, guided by X-rays and bony landmarks, to thermally coagulate dysfunctional tissues [4, 5]. In these early human studies, it was demonstrated that FUS can be used to selectively ablate targeted

khynynen@sri.utoronto.ca.

regions while sparing surrounding and overlying tissues. Since the integration of FUS with ultrasound imaging systems was first proposed in the 1970's [6], several ultrasound-guided devices have been clinically tested and have received regulatory approval for specific indications in different parts of the world [7, 8, 9]. In the early 1990's, FUS applicators were combined with magnetic resonance imaging (MRI)-guidance [10]. This approach has provided precise tissue targeting and exposure control, increased the effectiveness of the treatments, and resulted in approval from the Food and Drug Administration (FDA) for uterine fibroid (in 2004) and bone metastasis (in 2012) treatments [18, 11], with many other clinical indications currently under testing [12]. The first ultrasound-guided device [13] was recently approved by the FDA for prostate therapy in late 2015.

The FUS systems employed in early clinical studies under ultrasound or MR guidance [7, 14, 15, 16, 17, 8] consisted of single-element transducers, and therefore required mechanical translation for targeting and therapy delivery. However, it was soon realized that the treatment of many or large tumors would require greater spatial coverage than that provided by fixed-focus, single-element transducers. As a result, ultrasound transducer arrays comprising multiple elements were investigated for therapy [19, 20, 21, 22], though these early devices provided limited electronic control over the focal spots' shape and location. Phased arrays also allow wave-front distortions induced by acoustic propagation through heterogeneous tissues to be accounted for, which is not possible with single-element transducers and was critical for enabling the use of FUS therapy in the brain [23]. Although fully electronically-steered arrays have been used in diagnostic ultrasound for some time [24], there have been some major technical obstacles prohibiting their use in the context of therapy delivery (see section 3.1). However, these challenges have now been overcome, and it is possible to implement full-scale phased array systems for FUS therapy. We anticipate that, in the future, the full utilization of phased arrays will allow complete electronic control over the beam shape and location of the focal region, hugely improving FUS treatments for many indications.

The exploitation of microscopic gas bubbles as acoustic energy concentrators has uncovered many new opportunities for FUS therapy, but it also provides the problem of effectively controlling and monitoring the energy deposition. This is challenging due to the low acoustic powers delivered during these non-thermal treatments, which eliminates the possibility of using thermometry-based techniques for exposure control. During such treatments, the spatial locations and activity of these microbubbles need to be monitored to ensure the safety and efficacy of the therapy. As will be discussed below, recent research has demonstrated that this can be accomplished very effectively with passive ultrasound receiver phased arrays, and it is therefore expected that in the future, some FUS treatments will be optimally executed with combined phased arrays that can simultaneously transmit and receive ultrasound energy.

This review begins with a brief discussion of FUS and its effects on tissue (section 2). Section 3 covers the basic principles of therapeutic phased arrays, followed by a review of the different sonication patterns that are achievable with multi-element devices (section 4). Section 5 surveys the various imaging modalities used for FUS therapy guidance to date. The existing clinical and experimental image-guided phased array systems are summarized

in sections 6 and 7, respectively. Finally, some of the developing therapeutic applications of FUS are highlighted in section 8.

## 2. Basic Principles of Focused Ultrasound

### 2.1. Generation of an Ultrasound Field

The basic principles of ultrasound generation can be found in many text books (*e.g.* [25, 26]). Figure 1 illustrates a simple case of how ultrasound waves can be generated by a piezoelectric plate that has metal electrodes on both its front and back surfaces. The electrodes are connected to a radio frequency (RF)-driving line that applies a time-varying voltage across the electrodes. Due to the inverse piezoelectric effect, the piezoelectric material expands and contracts in proportion to the applied voltage and generates a mechanical disturbance, at the frequency of the RF-signal, in the medium in contact with the front surface.

The fundamental resonance frequency of a transducer corresponds to the case where the wavelength in the piezoelectric material is equal to twice the thickness of the plate. When a transducer is driven at resonance, all of the reflected waves at the plate surfaces are in phase and a maximal acoustic output is achieved. Ultrasonic transducers can also be driven at odd integer multiples of their resonance frequency, though the electric-to-acoustic power conversion efficiency is diminished. For therapy transducers, a low-impedance backing (*e.g.* air) is commonly used to ensure that total reflection occurs on the back surface of the plate and that the majority of the generated energy is directed through the front of the transducer, providing maximal power output within a very narrow frequency bandwidth. The acoustic impedance of a piezoelectric material is typically high compared to biological tissue and coupling liquid, however, matching layers can be used to improve the energy transmission from the plate to the tissue. The matching layer thickness that maximizes the energy transmission is one quarter of the ultrasound wavelength in the matching layer material, and the optimal acoustic impedance is given by the geometric mean of the impedance of the piezoelectric material and of the load. It is also possible to manufacture devices that have a wider operating frequency range by using composite materials [27]. These materials contain, for example, small (compared to the wavelength) pillars of the piezoelectric material that are embedded in a softer polymer, resulting in a reduced acoustic impedance. Composite material transducers were originally developed for ultrasonic imaging purposes but have since found use in therapy [28] due to their increased operating frequency range and reduced lateral-mechanical coupling, which enables convenient multi-element array construction by simply patterning the electrodes [29].

Typically, the RF-driving line contains a signal source that generates the sinusoidal RF-signal at the transducer's resonance frequency. An amplifier connected to a dual-directional coupler and a power meter for monitoring the transmitted and reflected power amplifies this signal, which then propagates through a tuning network that matches the transducer's impedance to the output impedance of the amplifier at the resonance frequency. For multi-element phased arrays, each of the array elements is driven independently with its own driving line.

### 2.2. Focusing of Ultrasound Waves

In order to overcome the signal losses in tissue due to acoustic absorption and scattering [30], and concentrate acoustic energy into a small volume, ultrasound beams can be focused. This can be accomplished using spherically curved transducers [31], acoustic lenses [32, 33], reflectors [34], or phased array applicators. By using large (compared to the wavelength) sources, ultrasound fields can be focused to a spot with a focal size on the order of the wavelength. The size and location of the focus can be controlled by varying the geometry (*i.e.* aperture and curvature) and operating frequency of the transducer (Figure 2). For spherically-curved transducers, the focus is ellipsoidal and has dimensions that can be approximated by simple formulae [26]: the lateral full-width at half-maximum is given by $1.4,\lambda\times f$-number, and the depth of field in the axial direction is $7.2,\lambda\times(f\text{-number})^2$ , where $,\lambda$ is the acoustic wavelength, and the *f*-number of a transducer is defined as the ratio of the focal length to the effective aperture diameter. Therefore, if large aperture transducers are used, focal spot diameters on the order of 1-3 mm and lengths of approximately 5-30 mm can be achieved deep within the body at clinically-relevant frequencies. Due to the high degree of focusing, the energy deposition in the near- and far-fields is small in most cases (Figure 2).

### 2.3. Ultrasound-Tissue Interactions

Ultrasound can induce a variety of biological effects on the vasculature and tissue depending on the specific acoustical parameters (*e.g.* frequency, pressure, pulse length, pulse repetition frequency) employed. The mechanisms of action of ultrasound-induced bioeffects can be broadly classified into thermal and mechanical categories, though therapies are often based on combinations of the two. The biological effects of ultrasound have been widely reviewed in the literature [35, 36, 37], and are therefore only briefly covered here.

Depending on the exposure conditions and tissue properties, ultrasound can induce local temperature elevations that can be employed in two different regimes of thermal therapy. The first is hyperthermia, where long acoustic exposures are used to induce and maintain mild temperature rises (absolute temperature range: 40-45°C) for several minutes to hours. Hyperthermia can elicit a variety of cellular and physiological effects in both normal and tumorous tissues that can either lead to cytotoxic effects directly or can be used as adjuvants to other therapies [38]. The second form of ultrasound-mediated thermal therapy is ablation, where short, higher power ultrasound exposures are used to raise the absolute temperature of tissue to 55-60°C for time scales on the order of seconds to minutes, leading to rapid cell death via thermal coagulation [39].

Acoustic cavitation can be induced within tissue and the vasculature through direct nucleation of bubbles from the absorbed gasses present *in vivo* during the rarefactional phase of high amplitude, pulsed exposures [40]. For example, in cavitation-cloud histotripsy, high intensity, low duty cycle ultrasound exposures are employed to generate and sustain dense bubbles clouds, through shock-scattering [41] or direct excitation [42], ultimately resulting in tissue homogenization. Boiling histotripsy is a separate approach for tissue fractionation [43], which can occur in the absence of thermal effects [44], and appears to involve ultrasonic atomization [45]. Alternatively, encapsulated microbubbles [46, 47], or

pre-cursors [48], can be introduced into circulation to provide cavitation nuclei and substantially reduce cavitation thresholds in tissue. Ultrasound-induced cavitation, with or without the use of injected agents, has a variety of therapeutic applications (see reviews [49, 50, 51, 52, 53, 54]).

Ultrasound beams generate a radiation force in the direction of acoustic propagation, through momentum transfer to the propagation medium, resulting in tissue displacements and acoustic streaming in fluid-filled cavities [55]. Most notably, it has been shown that radiation force effects can trigger premature heartbeats [56], promote the movement of microbubbles [57, 58] and thrombolytic agents [59] to vessel walls and their subsequent tunneling into gels and fibrin/plasma clots, and increase the clearance of both residual kidney stone fragments after lithotripsy [60, 61] and of cavitation nuclei to enhance histotripsy efficiency [62].

## 3. Ultrasound Phased Arrays

### 3.1. Introduction and History of Therapy Phased Arrays

When an ultrasound transducer has a size that is equal to or smaller than half of the wavelength ($\lambda/2$) in the medium of interest, it emits a spherical wave that propagates amongst the entire half-space in front of it. By placing many small elements in a row, and by controlling the timing of the transmitted wave from each element so that the individual waves arrive in phase at the desired location, an acoustic focus can be created. With such linear one-dimensional (1D) arrays, the focal location can be scanned within the axial plane of the transducer by adjusting the driving phases of the RF-signals, facilitating electronic beam focusing (Figure 3). By making the array two-dimensional (2D), full three-dimensional (3D) control of the ultrasound beam can be achieved, enabling the generation of multiple simultaneous focal spots, focal rings, and pressure minima (see section 4.3). Phased arrays have been used extensively in radar and sonar technology [63, 64] and have more recently been employed for diagnostic ultrasound imaging [24, 65]. The use of phased arrays in the context of therapeutic ultrasound was first proposed in the early 1980's [66] for controlling the focal depth in hyperthermia treatments with a concentric ring array.

There have been some major challenges in implementing fully steerable arrays for high-power therapy applications and, so far, they have not been fully utilized for this purpose. To have a full (*i.e.* $2\pi$ steradian) steering range, the transducer element center-to-center spacing needs to be less than or equal to half of the wavelength ($\lambda/2$) corresponding to the driving frequency in the medium of interest. This condition is relaxed to an element spacing of $\lambda$ in the case where only focusing along the central axis of the array is needed. With larger element sizes, and hence greater element spacings, the waves from individual array elements can form grating lobes due to constructive interference occurring at locations other than the desired focus (Figure 4). Thus, for a given array aperture, the operating frequency places an upper bound on the size of individual array elements, and consequently a lower bound on the number of elements, if a full steering range is desired. However, focusing acoustic energy deep into the body requires large geometric gains between the transducer surface and the focus, particularly when higher frequencies are employed since the effects of attenuation in biological tissue become more pronounced [67]. As a result, the individual transducer sizes

needed for therapy are typically much larger than those used in diagnostic ultrasound. Additionally, for a fixed driving frequency, the electrical impedance of a transducer increases as its size is reduced, and thus the delivery of adequate RF power to small elements becomes challenging. Moreover, the conversion efficiency of RF to acoustic energy diminishes with decreasing element size. These factors all favor the use of larger elements for therapy arrays and, as a result, it has not been possible to deliver sustained high powers from fully electronically steerable (*i.e.* λ/2-spaced) arrays. Furthermore, each transducer element needs to be connected to its own individual driving circuit, resulting in a substantial interconnect problem for arrays containing a large number of elements. In the following section, a brief overview of the current solutions to these issues surrounding high powered, densely populated phased arrays will be provided.

### 3.2. JD Arrays

The annular, or concentric ring, array design provides the ability to move the focal spot along the axis of the transducer and only requires one RF-driving line per ring, thus effectively reducing the complexity of the array to lD. Concentric ring arrays have been proposed for imaging [68], and are used for controlling the focal depth in an endocavity FUS prostate treatment system [69, 70]. Linear 1D arrays can steer the beam in the axial plane of the array, and have also been proposed for endocavity applications [71, 72, 73]. For completeness, it is worth noting that 1.25D, 1.5D, and 1.75D arrays (for definitions, see [74]) have also been proposed for use in therapy arrays [74, 75, 76].

### 3.3. 2D Large Element Arrays

The requirement of having a center-to-center element spacing of less than or equal to λ/2 can be relaxed by making the array curved and restricting the focal steering to regions in proximity to the geometric focus. Spherically curved sector arrays and spherically focused arrays with large elements have been proposed to increase the focal size and provide multi-focus capabilities [20, 77, 78, 79]. The early experimental arrays for thermal FUS surgery demonstrated the practicality and benefits afforded by the increased focal volume [21, 79, 80, 81, 29]. The first clinical MRI-guided uterine fibroid treatment device [18] was based on the design of these early prototype arrays.

### 3.4. 2D Fully Electronically Steerable Arrays

**3.4.1. Sparse Arrays—**An array design method that has been used effectively in antenna arrays to reduce the number of driving lines is to use small array elements, but to populate only a fraction of the total array surface in a random manner [82, 83, 84]. The randomness of the element locations mitigates the formation of grating lobes by incoherently distributing the off-focus energy within the field. Random sparse arrays have since been proposed for both diagnostic [85, 86, 87] and therapeutic [88, 89, 90] ultrasound arrays, and are capable of providing acceptable focal quality (Figure 5). A more recently developed MRI-guided FUS device for clinical uterine fibroid treatments employs a spherically curved, random sparse array design with large elements [90]. Indeed, a more robust alternative to the random array design is to use ultrasound field simulations to optimize the element distribution to maximize array performance [91, 87, 92], for example, by minimizing grating/side lobes or

maximizing the allowable steering range. Computer simulations [93] can also provide useful insights related to optimal array driving frequencies for specific applications [21, 94, 95].

The primary cost associated with sparse arrays is that energy is lost from the main lobe of the array's diffraction pattern and deposited away from the focus. With random and simulation-optimized phased arrays, this energy is incoherently distributed amongst a large volume, thereby minimizing the formation of local hot spots in tissue. The reduction in focal intensity is proportional to the transducer surface area that is not emitting ultrasound [96]. Therefore, more total energy is required from a sparse array to achieve the same acoustic intensity or temperature elevation at the focus than a fully populated array, all else equal. This is a significant drawback for thermal surgery treatments since the extra energy is transmitted through the superficial tissues, causing increased near-field heating that limits the rate of ablation (Figure 5) [96, 97]. However, sparse arrays may be useful for cavitation-based therapy [98], where the required time-averaged powers are much lower, meaning that superficial tissue heating is no longer a limiting factor. Sparse receiver arrays have also found application in passive acoustic imaging (see section 5.2) for cavitation mapping [99, 100, 101].

**3.4.2. Large Number of RF-Drivers and Interconnects—**Our lab has explored two ways to economically solve the need for thousands of RF-drivers and interconnects in ultrasound therapy phased arrays. First, it is well known that the phase resolution of the driving signals does not need to be very precise, and that good focusing can be achieved with low-resolution signals [102, 71]. Indeed, this same outcome was discovered when flat lenses were designed for ultrasound therapy [103]. As a result, only a subset of high-power RF-drivers need be used, combined with switches to connect each of the array elements to the RF-line with the closest phase to that which is needed. A combined simulation and experimental study [104] demonstrated that this indeed is possible, and that good electronic steering can be achieved with only four driving lines (Figure 6). The other advantage of this driving method is that the elements are connected in parallel, effectively increasing the transducer element area and reducing its electrical impedance. Such an approach could be easily implemented with CMUT arrays (see section 3.4.4).

Another approach for reducing the large number of interconnects, which offers more flexibility, is to take advantage of modern electronic device manufacturing and use application-specific integrated circuit (ASIC) technology to design custom circuits in order to reduce the cost and size of the drivers, as has been done with the electronics in diagnostic ultrasound systems [105]. The downside of this method is the initial high cost of reaching a satisfactory chip design and the subsequent time and cost required if any modifications are needed. However, the advantage is that the full potential of phased arrays can be achieved at a relatively low manufacturing costs once a satisfactory design has been achieved. Both the reduced phase resolution method and ASIC technology can be combined to offer practical solutions for fully electronically steerable arrays.

**3.4.3. High Electrical Impedance—**Our lab has provided a solution the problem of high electrical impedance by placing the metal electrodes on the sides of the transducer elements instead of on their front and back surfaces (Figure 7). This method increases the electrode

surface area and reduces the thickness of the transducer material in between the electrodes, both of which act to reduce the element's electrical impedance. However, instead of driving the element at the frequency corresponding to the thickness of the material between the electrodes, the driving frequency is instead selected to be that which corresponds to the length of the element in the direction parallel to the electrode surfaces. Since an element's resonance frequency is primarily determined by the thickness of the transducer material in the vibration direction, the impedance can be tuned by changing the thickness of the transducer element between the electrodes while keeping the frequency constant. This allows transducers to be manufactured at the optimal impedance for the driving electronics. We first demonstrated this lateral mode coupling method with cylindrical elements [106, 107] and subsequently with a lD phased array made out of multiple plates [108]. More recently, a 2D planar array was constructed using this technology [109].

**3.4.4. Capacitive Micromachined Ultrasonic Transducers (CMUTs)—**Ultrasound can also be generated using a capacitive method where the transducer is formed by a back plate, a cavity, and a thin metallic membrane electrode that can stretch and be displaced closer to or farther away from the back plate in response to an applied voltage [110]. Micromachining methods can be used to build these transducers so that large arrays can be manufactured at relatively low costs, and since silicon is used for manufacturing these devices, the driving electronics can be built right into the back of the array. This approach has been successfully used in diagnostic imaging [111, 112] and more recently in catheter-based devices for thermal ablation [113]. CMUT technology holds a lot of promise for high-power therapy devices since it solves most of the challenges related to phased arrays, such as the interconnect problem.

### 3.5. Performance Measurements of Phased Arrays

The performance of phased array transducers can be evaluated using standard experimental methods commonly used for single-element transducers [114]; radiation force balance measurements can be used to quantify the total acoustic power of the array, while hydrophone measurements can provide additional information regarding the spatiotemporal pressure field generated by the device. It has been demonstrated that hydrophone measurements of a pre-focal 2D planar field can be used to infer the velocity distribution on the transducer surface as well as the pressure field in the focal region using back- and forward-projection methods, respectively [115, 116, 117, 118]. This combined measurement and modeling approach has several uses as a quality assurance tool, but of particular importance to phased arrays, back-projection onto the surface of the transducer can be used to determine the functionality of individual array elements [115, 116, 117, 118]. This approach can be used to test if any significant phase or amplitude variations exist from element-to-element, which could subsequently be compensated for in order to improve the overall acoustic field generated by the array.

## 4. Phased Array Sonication Patterns

Phased arrays provide unparalleled flexibility in tailoring the acoustic field to be optimal for different treatment situations. In the following section, some of the approaches explored to date will be reviewed.

### 4.1. Single Focus Scanning

The simplest option for exposing a target volume that is larger than the acoustic focus is to scan the beam to provide the desired spatial coverage (Figure 8). Although in many cases mechanical scanning of a fixed-focus, single-element transducer is capable of providing the increased spatial coverage needed to treat large volumes, electronically steered phased arrays can do it faster and with more control over the energy deposition [119, 120]. For thermal FUS therapy, simple circular patterns simulating those used in the early hyperthemia treatments [121] have been proposed. When using this approach, the focal spots should be scanned fast enough to avoid excessive temperature fluctuations [122] such that the thermal dose can be accurately calculated based on temporally sparse temperature sampling (on the order of seconds per image [123]). For the rapid thermal ablation of large volumes, this means that at each focal spot the sonications should be repeated at a period of approximately 600 ms, and they should be positioned close enough to each other such that a uniform thermal dose is delivered [81].

For FUS treatments that utilize preformed microbubbles, repeat sonications are performed after new bubbles have been perfused into the focal volume. For ultrasound-mediated blood-brain barrier (BBB) opening, most of the experiments reported to date have used a repetition interval of 1 s [46], although longer intervals may provide better bubble recovery [124]. For cavitation-cloud histotripsy, the repetition time is typically shorter (1-100 ms), while for boiling histotripsy sonications a 1-2 s interval seems adequate [54]. Similarly, for tissue vaporization [125] the focal location could be held constant for the 0.5 s needed to form a cavity before moving on to the next location.

### 4.2. Aberration Correction

An important feature of phased arrays is that they can correct for wave-front aberrations induced during acoustic propagation through heterogeneous media by varying both the phase and amplitude of the individual transducer elements, which is particularly important in transcranial [126, 127, 128, 129] and transcostal [130, 131, 132] applications. The necessary aberration corrections can be obtained using various methods, including acoustic measurements with a small transducer [127], hydrophone [126, 128, 133], or acoustically-stimulated microbubble [134, 135, 136, 137] placed near the desired focal point, pitch-catch [138] or pulse-echo [139] ultrasound measurements, MR acoustic radiation force imaging (ARFI) [140], as well as patient-specific ultrasound propagation simulations using MRI [141, 142, 143] or computed tomography (CT) [144, 145, 146] scans to define the computational domain. Such imaging-based approaches have been proposed to determine which array elements should be switched off during transcostal FUS treatments to avoid overheating the ribs [147, 148].

### 4.3. Advanced Sonication Patterns

Phased arrays can also use the amplitude and phase of the driving signals to change the focus shape or generate multiple foci simultaneously (Figure 9). Cain and Umemura were the first to exploit this capability of ultrasound phased arrays to generate a ring-shaped focus [149, 20], and ultrasound field optimization methods were subsequently developed to allow optimal field generation [150, 151]. This method has been studied for both hyperthermia [150, 151, 152, 153, 154] and thermal surgery applications [155, 21, 120], and more recently in the context of neuromodulation [156]. Furthermore, the quick scanning of several multi-focus patterns could be used to generate optimal heating patterns [81]. The advantage of multi-focus approaches over scanning a single focus is that the peak acoustic pressure is reduced; an important feature if inertial cavitation is to be avoided. Finally, the control over the phase and amplitude of the driving signals of large aperture phased arrays also allows pressure field minima to be generated at critical locations where energy deposition should be minimized [157], which may have use in specific applications of transcranial FUS brain therapy [158].

## 5. Image Guidance

The non-invasive nature of FUS therapy necessitates the concurrent use of technology that is capable of performing precise ultrasound beam targeting, therapy monitoring, and post-treatment evaluation. To date, three major medical imaging methods have been used for these purposes: X-ray/CT, ultrasound, and MRI (see reviews [159, 12, 160]). For image-based targeting, the chosen modality should be able to ensure correct patient positioning, clearly delineate the target region, identify an appropriate acoustic window for the beam path through the intervening tissue, and locate the focal zone within the target tissue. For treatment monitoring, it is necessary to detect and confirm the target location prior to producing irreversible damage, monitor or predict tissue damage and lesion formation as it occurs in the target zone, and provide feedback with regards to potential unintended heating or tissue damage outside the intended target zone. Finally, the ability to evaluate the therapeutic effects after completion of the ultrasound exposures is also important from a treatment verification perspective. The following section will review the different medical imaging methods used for FUS therapy guidance, and discuss the benefits and drawbacks of each modality in this context.

### 5.1. Magnetic Resonance Imaging Guidance

MRI has two major advantages for guiding FUS therapy compared to other alternative methods. First, its excellent soft-tissue contrast allows for the accurate delineation and boundary mapping of both the intended target region as well as the treated volume post-therapy. Second, MRI can map ultrasound-induced temperature elevations in tissue (see reviews: [161, 162]), and it can do so with adequate sensitivity such that the focal temperature elevation can be detected and localized at exposure levels that do not cause any harm to even the most thermally sensitive tissues [163]. This unique ability can be utilized to ensure precise targeting before applying therapeutic sonications, ensure accurate mapping of the thermally coagulated tissue volume, as well as to monitor heating in surrounding tissues outside of the intended treatment zone. Although several MR parameters are temperature

sensitive, at present only MR-thermometry based on the dependence of the proton resonance frequency-shift on temperature [164, 165] has been shown to be capable of quantitative temperature monitoring during clinical treatments. This approach has been shown to have good temperature sensitivity and linearity in most tissue types, but is highly sensitive to tissue motion and is not temperature dependent in either fat or bone [166, 167]. MR-ARFI has also been proposed as a method for detecting the focal spot location *in situ* during FUS treatments [168].

In MR-thermometry, multiple temperature maps are obtained during each sonication to provide a time history of the temperature elevation that can be used to calculate a thermal dose map [169], which gives an indication of the tissue effects resulting from the thermal exposure [170]. The manner in which individual sonications are placed to cover a given treatment volume can vary from inducing sequential, partially overlapping focal volumes to more complex patterns that permit cooling of tissue between sonications. The initial implementations of MR-thermometry for monitoring therapy required operators to obtain temperature maps at each location both to ensure that sufficient heating occurred and to permit adjustment of sonication parameters between locations. Since then, a number of more sophisticated closed-loop feedback control approaches have been proposed and demonstrated through simulations and experiments [171, 172, 173, 174].

At the end of thermal FUS treatments, the ablated tissue is most commonly mapped through the use of contrast-enhanced $T_1$-weighted imaging, which can detect perfusion-deficient regions indicative of vascular stasis [175, 17, 18], though both tissue stiffness measurements via MR elastography [176] and diffusion-weighted MRI sequences [177] have also been proposed for this purpose. Additionally, $T_2$-weighted imaging can be used to detect any cytotoxic edema resulting from FUS therapy [178, 179]. A case example of uterine fibroid treatment via MR-guided FUS ablation is shown in Figure 10, illustrating the use of temperature monitoring to determine the ablation region, followed by treatment confirmation with contrast-enhanced imaging. MRI has several additional uses for monitoring non-thermal, FUS-induced BBB opening treatments: contrast-enhanced $T_1$-weighted imaging is used to detect changes in BBB permeability [46], while $T_2^*$- or susceptibility-weighted imaging can monitor for the presence of hemorrhage [180].

Despite the clear advantages of MRI as a modality for guiding FUS therapy outlined above, it carries with it considerable purchasing and maintenance costs, which may therefore limit its immediate use primarily to Western countries.

### 5.2. Ultrasound Guidance

Despite the fact that ultrasound imagmg is largely inferior to MRI in terms of soft tissue contrast, it is the most widely used modality for guiding FUS therapy when the number of treated patients is counted globally. The main reasons for this are its low cost, compact size, portability, high temporal resolution, and rapid data acquisition capabilities. Ultrasound imaging also allows for monitoring of cavitation events over short timescales in the absence of thermal effects, which is not possible with current MRI methods. Indeed, the current clinical FUS systems for brain therapy use several hydrophones to monitor the generated acoustic activity to ensure that the inertial cavitation threshold is not reached [181], in order

to avoid potential hemorrhaging and other unwanted effects [182]. However, unlike MRI, ultrasound imaging is currently unable to provide reliable and precise temperature mapping during FUS exposures. Researchers are actively exploring the feasibility of using a variety of diagnostic ultrasound-derived parameters (*e.g.* absorption, speed of sound, coefficient of non-linearity) for temperature monitoring, with success so far in phantoms and pre-clinical experiments, though clinical demonstrations have not yet been realized [183]. Tissue echogenicity has been proposed as a method to indicate lesion formation [184], but its correlation with the coagulated tissue volume has not been precise. Nevertheless, changes in tissue stiffness resulting from thermal coagulation can be measured using various ultrasound-based elasticity methods [185, 186, 187, 188, 189], and hence may prove to be a useful alternative to temperature for the monitoring and control of thermal FUS treatments. Finally, contrast-enhanced ultrasound can be used to assess non-perfused regions as a means of detecting patient response to thermal FUS therapy [190].

In order to effectively harness acoustic cavitation for therapeutic purposes, the distribution of active microbubbles needs to be monitored and controlled during treatment. In addition, information regarding the response of the bubbles to the ultrasound exposures should be monitored to assure that the desired bioeffects are produced [191, 192, 193, 194]. Therefore, ultrasound imaging methods will play a key role when cavitation-based therapies are translated into the clinic, since they are the only means for effectively providing all of the aforementioned information. Traditional pulse-echo ultrasound imaging can be used to localize bubbles using specialized imaging sequences [195, 196, 197]. Alternatively, since FUS therapy exposures are already transmitting ultrasound into the tissue, the backscattered components of the therapy pulses can be detected, processed using passive beamforming, and used for imaging and control purposes. This imaging approach, termed passive acoustic mapping (PAM), has been proposed for acoustic source localization [198] as well as for seismic imaging [199], but has more recently been investigated by many research groups for monitoring cavitation activity during the application of FUS [200, 201, 202, 136, 203, 204, 101]. Although the majority of the experiments to date have used commercial 1D linear phased arrays for PAM that are separate from the therapy applicator, it is expected that a full integration of the therapy and imaging arrays will provide the best results. With integrated arrays, the spectral information of the backscattered signals can be collected and used to control the subsequent exposures so that the desired biological endpoints can be consistently reached [205, 206]. Furthermore, integrated arrays are particularly attractive for brain applications, since the large-aperture hemispherical arrays used for therapy provide optimal imaging resolution and sensitivity for PAM [199], and enable 3D cavitation mapping without mechanical translation of the array [101].

### 5.3. X-ray and Computed Tomography Guidance

X-ray imaging can be used to determine target locations for FUS therapy relative to anatomical landmarks such as bones and other easily visible structures present on imaging. Indeed, it was the first imaging modality used for guiding FUS interventions; X-ray imaging was effectively used by Fry *et al.* to target structures in the brain during early experiments of FUS therapy on patients with Parkinson's disease and various other neurological afflictions [4, 5]. Fluoroscopy has been investigated for guiding ultrasonic catheter systems to the

appropriate anatomical site [207, 208]. X-ray guidance is also used during shock-wave lithotripsy for kidney stone disintegration [209]. CT is used for treatment planning of FUS brain treatments (see section 4.2): CT-based aberration corrections are used in the current generation of clinical FUS brain devices [210], and have also been shown to improve image quality during transcranial PAM [100, 211, 212, 146]. Finally, CT imaging also has the potential of detecting thermal effects during FUS treatments through the dependence of tissue density on temperature [213]. However, compared to other imaging modalities, X-ray and CT imaging suffer from relatively poor soft-tissue contrast and can deliver high radiation doses to both the patient and medical technician.

### 5.4. Hybrid Guidance Methods

Perhaps the most effective, yet expensive, method for guiding FUS treatments would be to combine the best features of each imaging modality and use them for therapy monitoring and control. For example, combined MR and ultrasound ARFI during thermal FUS therapy has been demonstrated in animal studies [214], with MR-thermometry and PAM having also been shown to be feasible simultaneously [215]. In the future, it is expected that a fully-integrated transmit/receive phased array could be used with simultaneous MR imaging and thermometry. Ultimately, for cancer treatments, one could envision using a transmit/receive ultrasound phased array guided by a combined MRI-positron emission tomography (PET) system [216] for molecular imaging and targeted drug delivery. Such a composite system could utilize the superb soft-tissue contrast, spatial resolution, and temperature mapping provided by MRI, together with the high sensitivity to radioactive tracer molecules offered by PET, combined with the ability of PAM to map the locations and strength of the microbubble activity during FUS treatment.

## 6. Clinical Image-Guided Phased Array Systems

There are now several companies exploiting the therapeutic potential of FUS phased arrays, the majority of which are focused on device development for tissue ablation via ultrasound-induced temperature elevations. The basic approach for thermal FUS surgery is to point the focal zone to a location within the target volume, sonicate to coagulate the tissue and then move on to the next location, thereby accumulating damage in a conformal manner over the entire region of interest [217, 218]. In certain clinical systems, the focus can be spatially scanned during the exposures to increase the coagulated volume during each sonication [219, 220]. At each target location, acoustic intensities ranging from $10^3$-$10^4$ W/cm$^2$ are delivered, with dwell times on the order of 1-100 s to allow the overlying tissue to cool between successive sonications. In the following section, the commercially available image-guided phased array systems will be reviewed, grouped by anatomical target region in the body.

### 6.1. Pelvic

Uterine fibroids [221] (or leiomyomas) are remarkably common, benign, and often large tumors that can cause clinical symptoms that are so severe that surgical removal of the tumor is necessary. However, surgical resection can cause a large number of unwanted complications and is associated with long recovery times, even after minimally invasive

fibroid removal. Thermal ablation FUS therapy is a relatively new treatment approach for uterine fibroid surgery. There are currently two commercially available FUS phased array systems for uterine fibroid treatments [18, 219]. Both of these devices are guided by MRI and employ spherically-curved arrays with relatively large array elements, resulting in limited electronic focal steering capabilities. In these devices, which are described below, the phased arrays are mounted on mechanical translation devices that are built into the MRI bed. During treatment planning, the transducer is registered with the MRI coordinate system so that the computer-controlled positioning system can aim the acoustic focus by moving the transducer based on image-derived target locations. The transducer chamber is filled with liquid and covered with a thin plastic membrane for acoustic coupling.

The InSightec (InSightec, Inc., Tirat Carmel, Israel) fibroid system [18] employs a fully populated, hybrid sector-vortex and concentric ring phased array (12 cm aperture) design that allows the focal location to be controlled mainly in the depth direction with a small degree of lateral steering [20, 79]. The array has a total of 208 elements and operates at a frequency between 0.96-1.14 MHz. The system is mechanically positioned to aim the beam due to the limited steering range afforded from electronic focusing, and the device can also be rotated along two angular directions to allow the beam orientation to be controlled so that near- or far-field structures can be avoided. MR-thermometry is carried out during the ultrasound exposures for temperature and thermal dose monitoring [222, 177]. Initially, low-power sonications are conducted to determine the focal location and assess targeting accuracy, followed by additional sonications at therapeutic power levels once the targeting is deemed to be adequate. This latest generation of this device allows for interleaved exposures, allowing for a greater number of sonications to be delivered in the same treatment time [220].

The Philips (Philips Healthcare, Inc., Vantaa, Finland) fibroid system [219] also uses a spherically-curved, large element array (12-14 cm aperture) to allow for beam steering in the vicinity of the geometric focus. A random sparse array design [90] is employed to extend the focal steering range at the cost of increased near-field heating. The array consists of 256 elements, can be driven at frequencies between 1.2-1.45 MHz, and employs volumetric exposures controlled by feedback from MR-thermometry [174]. The current implementation of the controller is relatively straightforward: the array begins by sonicating at the geometric focus by scanning the focal volume around a 4 mm diameter circle, or treatment cell. When the temperature reaches a pre-defined target value the system is designed to terminate the sonication, though if a larger ablation volume is desired the scanning will continue with treatment cells of 8, 12, and 16 mm in diameter. Otherwise, if the target temperature is not reached within a given amount of time, the system is designed to terminate the sonication. The system also allows for fixed-power sonications without using the MRI-based controller.

Both of these systems have been shown to be effective in treating uterine fibroids using large focal spots. Clinical results have shown that the volume of thermal coagulation can be assessed by examining the non-enhanced volume in post-treatment, contrast-enhanced MRI scans [223]. This non-enhanced tissue volume has been shown to correlate with both the reduction of fibroid volume over time as well as the duration of symptom relief [222, 224]. The most notable benefit of FUS treatment for uterine fibroids has been the short recovery

time (one day away from normal activity, on average [225]), due to the fact that the treatment is completely non-invasive. This compares favorably with standard treatment approaches, such as hysterectomy and myomectomy [226]. However, the treatment times for large fibroids are still long and only a relatively small proportion of patients are suitable for FUS treatment with the currently available clinical systems. Fibroids that are highly perfused, indicated as hyperintense in pre-treament $T_2$-weighted imaging [223], or that have low acoustic absorption, are difficult to heat [227]. Further complications can arise from the location of the fibroid: fibroids located too close to the spine or without an appropriate acoustic window (*e.g.* fibroids located behind bowel, thick fat layers, or large scars) are typically ineligible for treatment [220]. However, it is expected that at least some of these limitations could be overcome using a more optimal phased array design [228].

### 6.2. Bone

Metastatic bone tumors, which arise in over 50% of all cancer patients [229], with approximately 50-75% of these suffering from severe pain that is difficult to control [230], are a significant quality of life issue for advanced cancer patients. The high rate of ultrasound absorption in bone makes these tumors easy to heat at low acoustic powers [231]. Both of the FUS fibroid systems described above have been clinically tested for the treatment of pain caused by bone tumors, showing a quick and lasting impact on pain scores [232, 233], with similar pain relief observed in treating back pain using these same devices [234]. However, patient positioning on both systems is not straightforward, particularly as many patients have difficulty lying on their painful bone tumors. For this reason, InSightec has developed a dedicated phased array system for bone metastases, which consists of 1000 elements operating at a frequency of 550 kHz, that can be strapped on the patient on top of the tumor [235]. The system has a focal steering range of approximately 30 degrees, and focuses the beam past the tumor, exploiting the high ultrasound absorption in bone and the large beam diameter in the near-field region to increase the ablated bone surface area.

### 6.3. Prostate

Prostate cancer is the most diagnosed cancer type in men, and despite the existence of many effective treatments, it is still the third leading cause of death among men from cancer in the United States [236]. Although surgical removal of the prostate or radiation therapy can effectively control the disease in many men, these treatments are associated with undesirable side-effects that reduce the patients' quality of life [237]. Indeed, a method for image-guided, precise, and non-invasive ablation of prostate tissue would be a desirable treatment option for these patients. The first phased array used for FUS therapy in the prostate was developed by EDAP TMS (EDAP TMS, Lyon, France), and exploits a 3 MHz, 16-element spherically curved array (5.6 cm aperture) with a concentric ring design to control the focal depth [69, 70]. The transrectal device contains a central disk void within which an ultrasound imaging probe is placed for treatment guidance [70]. The long-term results from this device's single-element predecessor are comparable with other alternative therapies [238], but there are significant side-effects associated with the procedure, which could potentially be reduced or eliminated with online temperature monitoring and control. Although there is currently no published clinical data on the use of the new phased array applicator, it is expected to improve upon the previous fixed-focus device by expanding the

size range and therefore number of treatable prostates, providing a more homogeneous ablation region, and reducing the length of the procedures.

InSightec has developed a transrectal phased array that aims to minimize the shortcomings of the previously described prostate device by employing MRI-guidance and thermometry. The array contains 990 elements, operates at a frequency of 2 MHz, and is placed in the rectum in an inflatable water bolus similar to the ultrasound-guided array described above. The device is mechanically moved in the length direction and rotated to aim the focal volume, while the depth of the focus and its size can be controlled electronically to some degree. The clinical feasibility of this approach has been demonstrated in a limited number of patient treatments [239], though more extensive clinical testing needs to be carried out to determine the clinical effectiveness of the device.

### 6.4. Brain

Since invasive interventions in the brain can be associated with detrimental side effects and complications, completely non-invasive approaches for neurological disorders have a particularly special appeal. However, there are two main obstacles for using FUS in the brain: first, the high acoustic attenuation of skull bone combined with the large specular reflections occurring at the inner and outer skull surfaces, as well as within the bone itself, act to reduce the amount of transmitted energy [240] and can cause extensive heating of the bone [241, 242]. Second, the variable structure, thickness, and density of the skull bone, together with the large differences of longitudinal sound speed in bone compared to the surrounding soft tissues, make the skull act as a defocusing lens, shifting and diffusing the focal energy deposition to a degree that trans-skull tissue ablation was not feasible during early investigations [2]. After these early experiments, research was conducted to measure the acoustic properties of skull bone [240], and subsequent feasibility studies demonstrated that low frequency focusing through human skull bone was possible in some instances, and that enough energy could be transmitted to focally ablate brain tissue [243]. Around the same time, it was demonstrated that small-element, linear 1D ultrasound arrays could correct the skull-induced beam distortion based on measurements with a small hydrophone [126] or emitting transducer [127] at the focus.

The potential feasibility of through-skull FUS therapy became apparent with the demonstration that large-element, high-power 2D arrays can also correct the focal distortion and deliver enough energy to ablate brain tissue [128]. This study, along with subsequent simulation [244, 245] and experimental [246, 247] investigations, showed that large hemispherical arrays covering most of the available skull surface may be able to thermally ablate deep brain tissue. It was also shown that enhancing focal energy absorption through the use of cavitation bubbles could potentially provide the gains needed to reach the whole brain [248]. However, the other key development needed was the ability to predict the necessary phase and amplitude corrections for the phased array elements non-invasively. This was first attempted by using MRI-derived skull thickness information [141], but eventually both the skull geometry and density obtained from high-resolution CT scans was needed to reliably focus through the skull [144, 145]. This required extensive experiments to determine the human skull properties (*i.e.* longitudinal sound speed and attenuation) as a

function of the skull density [249], which have since been extended to include the dependence on the ultrasound driving frequency [250]. Cumulatively, these research findings were the basis of the current clinical brain treatment device [251]. Although more advanced methods for trans-skull focusing have been investigated (see section 4.2), the current clinical systems still use CT-derived information for treatment planning.

The current clinical brain device, made by InSightec, is fully populated and has 1024 ultrasound transducer elements on a hemispherical surface (30 cm aperture) placed around the head of the patient (Figure 11). The array operates at frequencies between 650-720 kHz, which is within the range of frequencies that was shown to provide optimal thermal gains through human skull bone [245, 246]. A rubber membrane is placed around the patient's head and fixed to the array to allow cooled, degassed water to be circulated around the head. The circulating water serves two purposes; it acoustically couples the ultrasound beams to the head and acts to cool the skin and the bone to avoid overheating during the exposures [252, 253]. During FUS brain treatments, the patient is positioned in the MRI scanner with the array in place, and 3D $T_2$-weighted imaging of the head is performed. Based on these pre-treatment images, the array is mechanically moved so that the center of the hemisphere, and thus the geometric focus of the array, is roughly aligned with the target volume. Next, pre-treatment CT scans of the skull are super-imposed over the MR images so that the two datasets can be registered, and the CT data is then used to calculate the phase and amplitude corrections needed for focusing the beam to the target location of interest. Low-power sonications are delivered to check the focusing quality and determine if the generated hotspot is located at the intended target, or whether further adjustments are needed. Once the target and hotspot are aligned, the power is increased and the sonications are repeated until the desired temperature elevation (absolute temperature = 55-60 °C) is reached for irreversible thermal coagulation.

Although this technology was first tested for the treatment of tumors [210], currently the most experience is found in treating essential tremor, which has found good clinical success [254, 255, 256]. Ultrasound-induced thermal ablation in the brain has now been used in patients with tumors [257, 210, 258], chronic pain [259, 181], mental disorders [260], and Parkinson's disease [5, 261], with many other indications undergoing either pre-clinical or early-phase clinical testing [262].

### 6.5. Other tumors

As illustrated by the above examples, image-guided FUS phased arrays can be used to ablate a variety of tumors deep within the body in a clinical setting. Therefore, these general-purpose devices have been used to treat breast [263], liver [264], kidney [265], and other tumors [266]. Specialized phased array devices that are adapted to specific anatomical requirements have also been proposed. For example, two phased array systems have been proposed for breast tumor treatments [267, 268], both of which are entering clinical testing. Both of these devices suffer from limited electronic steering ranges and therefore rely on mechanical device translation for therapy targeting.

## 7. Experimental Image-Guided Phased Array Systems

The technical potential of FUS phased arrays has not been fully exploited in the current generation of clinical systems, and thus it is expected that large gains in treatment execution will be achieved by fully utilizing this technology. As explained previously, there have been some technological barriers preventing the full utilization of ultrasound phased arrays for therapy, but it appears that the development of fully electronically-steerable arrays is now feasible. In the following section, we will provide a brief summary of the research reports describing these more advanced phased array systems.

### 7.1. Pelvic and Abdominal

Although the current clinical treatments of uterine fibroids using FUS have shown great effectiveness to date, the treatments are slow and many patients do not pass the inclusion criteria (see section 6.1). A recent simulation study indicates that faster and deeper treatments could be executed if fully electronically-steerable arrays were to be used [228]. For treatment applications in the abdomen, such as liver and kidney tumors, the organs move so extensively and rapidly that fast steering is required in order to properly track this motion [269, 270], and the presence of the ribcage presents an additional obstacle. Several groups have developed phased array prototypes for transcostal FUS treatments [271, 272, 131, 132, 147], together with aberration correction techniques to focus behind the ribs (see section 4.2). However, it is expected that the implementation of fully electronically-steerable arrays will have a large impact on the execution of these thermal treatments by allowing sonications from a stationary device. This is particularly important for long-duration, mild hyperthermia treatments executed under MR-thermometry control for localizing drug therapy [273, 274, 275], where precise temperature information is needed over the entire therapy. Although such treatments have been successful for small animal tumors, either with an experimental scanning single-element transducer [273] or with the current limited steering phased arrays [274, 275], the heating of large tumors in a clinical setting would be greatly simplified if the transducer remained stationary.

### 7.2. Brain

Although the previously described phased array brain system developed by InSightec is currently in clinical use for ablative therapies, its electronic steering range is limited to focusing within a few centimeters from the geometric center of the device [262]. A lower frequency (220-230 kHz), fully-populated phased array system has also been developed by InSightec, which improves upon both through-skull energy transmission and the allowable steering range. This device has been mainly used for pre-clinical investigations, such as BBB opening [276], sonothrombolysis [277], mechanical [278] and thermal [279] ablation, and ultrasound-induced tissue disintegration [280]. However, this device is currently entering into clinical testing at our institution, in a trial to examine the safety of non-invasive doxorubicin delivery to the brain of glioma patients using FUS applied through the intact skull bone.

Researchers in France have developed several higher frequency (0.9-1 MHz) phased array prototype systems for brain therapy [89, 136, 281]. The current generation is fully populated

(23 cm aperture), consists of 512 elements, and has been tested with an *ex-vivo* human skull [282] and cadavers [283]. The *ex-vivo* human head experiments conducted with this device have reported good targeting ability but insufficient temperature elevations for successful tissue ablation [283].

At our institution, a phased array prototype with an increased steering range was achieved by fully-populating 1372 smaller cylindrical elements that could be driven at two main frequencies (306 and 840 kHz) onto a hemispherical shell (30 cm aperture) [107]. The use of cylindrical elements provided an opportunity to place ultrasound receivers in the middle of the transmitters, and in a later study a combined transmit/receive phased array was achieved by integrating a 128-element sparse receiver array within this transmit array [101]. The simulation-optimized sparse receiver array has been shown capable of localizing ultrasound-stimulated microbubbles through *ex-vivo* human skullcaps, using similar CT-based corrections to those used for transmit focusing [100], both within thin-walled tube phantoms and in an *in-vivo* rat model of BBB opening [211]. In a separate study, this array was found capable of imaging single microbubbles in 3D through an *ex-vivo* human skullcap, and by applying super-resolution techniques borrowed from optical microscopy the bubbles were localized with a spatial resolution beyond the diffraction limit (Figure 12) [137]. Therefore, this array has the potential to allow controlled bubble-based therapies with single-bubble precision. This array concept has since been extended to multi-frequency transmit/receive mode to provide more opportunities for bubble excitation and imaging (unpublished data).

Other research groups have developed multi-frequency phased arrays for brain applications. Researchers in Taiwan have developed a 256-channel system (12 cm aperture) for BBB opening applications which allows for simultaneous dual-frequency excitation with operational frequencies of 400-800 kHz [284]. Similarly, in the United States, a simultaneous multi-frequency (0.5-3 MHz) system (6.5 cm aperture) for histotripsy has been developed that can provide highly controllable, short (*i.e.* monopolar), high-amplitude ultrasound pulses for tissue disintegration [42]. The same group has also developed a large element, single-frequency (500 kHz) hemispherical (30 cm aperture) phased array prototype for transcranial histotripsy, which consists of 32 elements [285].

### 7.3. Cardiac

Cardiac ablation for the treatment of arrhythmia using ultrasound catheters was first demonstrated in animals over 20 years ago [286], but it has not progressed to clinical practice. However, there has now been renewed interest in developing intra-atrial catheters for either ultrasound or MRI-guided cardiac ablations. The main advantages of ultrasound devices compared to RF or laser-based devices are that thermal coagulation is more predictable, and it can be induced at greater depths using acoustic energy [287]. Small catheter-mounted, high-frequency CMUT phased arrays have been developed for this purpose and have shown to be capable of inducing thermal ablation [288]. Phased arrays may offer a less invasive approach via the trans-esophageal route routinely used for cardiac imaging. Simulation studies [289] have demonstrated the feasibility of this approach, and the practical development of such arrays has been promising [290, 291], however, fully electronically-steerable arrays for this purpose have not yet been realized.

### 7.4. Drug Delivery and Gene Therapy

Both cavitation- and hyperthermia-mediated approaches for targeted drug delivery and gene therapy (see section 8.2.2) require at least an order of magnitude lower time-averaged powers than those used for ablation, and therefore some of the issues associated with the use of phased arrays are reduced in severity. Recently, a combined therapy and imaging ultrasound phased array utilizing CMUT technology was developed and experimentally tested, showing promise for ultrasound-guided drug delivery [292].

### 7.5. Atherosclerosis

A recent simulation study [293] showing that FUS can be used to target and ablate atherosclerotic plaques, under diagnostic ultrasound guidance, has given hope that ultrasound can potentially modify the progression of such plaques *in vivo*. In this study, simulations were performed using a spherically-curved composite therapy array that had a limited electronic steering range

## 8. Future Developments

Both the current commercially available FUS technology and imaging-based treatment guidance methods are sub-optimal, and stand to benefit from the potential offered by fully electronically-steerable phased arrays. Similarly, the various interactions between ultrasound and biological tissues have not been fully exploited to date, and there are many new therapeutic opportunities in this regard. The following section will outline the expected future technical developments of image-guided FUS devices and potential new clinical applications of FUS therapy.

### 8.1. Technical Developments

With laboratory research demonstrating that the development of fully electronically-steerable arrays is feasible, one can expect several advances with the next generation of clinical image-guided FUS systems. First, with the elimination of mechanical parts to move the applicator, the reliability of the system should increase and the manufacturing costs should be reduced. Second, electronic focusing could be used to track moving targets at speeds that are not possible with current mechanical systems, which will be critical for ablating moving organs such as the heart and liver. Third, with large aperture, 2D phased arrays the ultrasound field for each sonication could be tailored to compensate for distortions induced by overlying tissues, minimize the pressure amplitude sensed by critical structures, and optimize the spatiotemporal distribution of the energy delivery, thereby reducing treatment times and providing better control over the treatment volume. Therefore, it is expected that the introduction of fully electronically-steerable phased arrays will make the majority of current treatments more effective and efficacious, as well as make other treatments feasible, thus taking a major step forward in the widespread clinical adoption of FUS technology.

### 8.2. Potential New Clinical Applications

**8.2.1. Vascular Applications—**Both thermal and cavitational bioeffects can have an impact on the vasculature within tissue [294]. For example, thermal coagulation of blood

vessels has been shown to result in complete cessation of blood flow [295, 296]. Ultrasound-induced hemostasis has been investigated in animal models for the emergency treatment of vessel rupture [297, 298] as well as for reducing bleeding during liver surgery [299]. Therefore, ultrasound phased arrays may have a future role in emergency medicine or in military medical care. Since portable devices are required for these applications, the FUS beams would likely need to be guided using ultrasound-based methods.

To date, acoustic cavitation has not been exploited for therapy delivery to the same degree as the thermal effects of ultrasound have been. Part of the reason for this is that cavitation interactions with tissue are more complex than thermal interactions, and furthermore, that there is not the same volume of basic science studies in the literature that can be used to guide treatment development. In addition, historically there has been a fear that cavitation could promote the spreading of cancer cells in tissue [300, 301, 302], though modern evidence now points to the contrary [303, 304]. Another valid concern is that cavitation can lead to large blood vessel ruptures and bleeding, which has been observed in some pre-clinical experiments [182]. However, over the past decade or so it has become evident that the majority of our understanding of acoustic cavitation in tissue has been based on studies that used ultrasound parameters either similar to or more severe than those used for inducing thermal effects, and that these exposure levels are much higher than those needed for inducing many desirable cavitation-mediated bioeffects. It has also been discovered that cavitation offers a wide range of biological effects on tissue and the vasculature, and that microbubbles are highly effective energy concentrators, which has enabled non-thermal FUS therapy with orders of magnitude-reduced energy delivery. This is especially important when treatments behind highly attenuating barriers, such as the skull or ribs, are considered.

There are many potential new applications of FUS that harness the interactions of ultrasound with microscopic gas bubbles, and indeed, cavitation-mediated therapy will continue to be an active area of both basic and clinical research. Perhaps the most exiting clinical applications that may arise from ongoing pre-clinical work are related to the ability of inducing focal and transient opening of the BBB non-invasively using FUS in combination with preformed microbubbles injected into circulation [46]. Extensive pre-clinical work has demonstrated that almost any molecule, particle, viral vector, or cell can be delivered to an MRI-identified location in animal brain using this technique [51, 305, 306, 307]. It has also been shown that the delivery of these agents can be effective in animal disease models, with huge potential for treating brain tumors [308, 309, 310], Alzheimer's disease [311, 312], and Parkinson's disease [313], just to name a few. The safety profile of FUS-induced BBB opening in large animals has been very promising [276], and the first human treatments have recently begun at our institution, in which we are non-invasively delivering doxorubicin to the brain of glioma patients to determine the clinical safety of the technique.

In embolic stroke patients, blood flow to part of the brain is blocked by a blood clot in the cerebral arteries. Ultrasound alone at high-pressure amplitudes has been used to disintegrate such clots in animal models, resulting in quick restoration of blood flow [314]. The same method may work for restoring blood flow in other blocked vessels, such as deep-vein thrombosis [315] or coronary artery occlusions [316], and may also aid in dissolving blood clots in the brain's ventricles [317]. An alternative approach is to use low-pressure amplitude

ultrasound in combination with thrombolytic agents (*e.g.* tissue plasminogen activator (tPA)) to accelerate blood clot lysis, the effectiveness of which has been demonstrated in human patients [318]. In the presence of lytic agents, the addition of contrast agent microbubbles could further reduce the pressures [319] and/or tPA doses [320] required for thrombus dissolution. Clinically, microbubble-mediated strategies have demonstrated enhanced recanalization rates in ischemic stroke [321] and are under continued investigation in the treatment of myocardial infarction.

Both FUS-induced BBB opening and sonothrombolysis treatments would greatly benefit from the use of fully electronically steerable transmit/receive phased array systems, both to increase the effective treatment envelope within the brain and to allow for the spatiotemporal monitoring of cavitation activity during the procedures. The use of a phased array system with a large steering range is particularly important for FUS treatments for both Alzheimer's and Parkinson's, which, particularly in late disease stages, are associated with neural degeneration over large cerebral volumes [322, 323]. Similarly, in sonothrombolysis for ischemic stroke, occlusions at superficial locations such as the posterior [324] or anterior [325] cerebral arteries could potentially be targeted with a large steering range device. Finally, as correlations between the acoustic emissions generated during both FUS-induced BBB opening [194] and sonothrombolysis [193] procedures and the associated treatment outcomes have been reported, the incorporation of the spatial information obtained from PAM into existing control algorithms [206] would greatly improve the practicality of such non-thermal FUS treatments.

**8.2.2. Drug Delivery and Gene Therapy—**FUS can be used to effectively localize and enhance drug delivery and gene therapy treatments through several mechanisms [326]. As discusssed in section 7.1, localized mild hyperthermia can release drugs from temperature-sensitive carriers within a confined, image-defined tissue volume. Here, the focal temperature elevation acts to increase the local blood flow of the tissue, further enhancing the drug toxicity in that region. In a similar fashion, elevated temperatures can be used to initiate focal gene therapy within the heated volume [327, 328]. Microbubbles can also be used for drug and gene delivery in several ways [329, 330]. For example, therapeutic drug-carrying microbubbles can be created by incorporating molecular payloads either onto the shell of the bubble or within its core. Upon ultrasound stimulation these molecules can be effectively released within the focal volume and subsequently delivered to the endothelial cells in tissue [331]. Alternatively, ultrasound-stimulated microbubbles can also be used to enhance the local permeability of blood vessel walls [332] and even cell membranes [333], which can be combined with the co-administration of various therapeutics for enhanced delivery. Finally, low-power ultrasound exposures combined with the injection of preformed microbubbles can activate sonosensitizer agents in a similar manner to how light activates photosensitising drugs in photodynamic therapy [334]. This approach is commonly referred to as sonodynamic therapy, which was initially proposed by Unemura *et al.* [335], and many research papers have since demonstrated its high effectiveness in animal tumor models using various therapeutic agents [336]. All of these ultrasound-mediated drug and gene treatments would benefit from precise control of the acoustic field, possible only by using phased arrays.

**8.2.3. Nerves—**Another promising use of FUS is for inducing either permanent or temporary nerve blockages [337], which has potential for applications in pain control [338], and may also be used to reduce muscle spasticity [339]. There has also been research demonstrating that ultrasound exposures alone can be used for neurological stimulation, inhibition, or modulation in humans [340, 341, 342]. Similarly, high-frequency ultrasound stimulation may have therapeutic potential for use in a retinal prosthesis [343]. The physical mechanisms underlying these findings are currently unclear, but the precise control of the applied ultrasound field provided by phased array applicators would make these treatments more practical.

**8.2.4. Cosmetic Treatments—**Since the early pre-clinical MRI-guided FUS studies it has been known that ultrasound can be used to thermally coagulate fatty tissues, and that the tissue is subsequently absorbed by the body. This ability of FUS to reduce fat was recognized by the cosmetic industry and is the most commercially successful use of FUS in humans, with several commercial devices on the market [344, 345]. Similarly, the use of focal thermal coagulation for the shrinkage of tissue has been investigated for skin-tightening using an FDA-approved device [346, 347]. Cosmetic treatments employing FUS might also benefit from phased array technology.

## 9. Conclusions

There is an increasing number of ways in which ultrasound can be used to manipulate biological tissue *in vivo*. FUS provides a way to deliver ultrasound exposures deep inside the body under image-guidance for precise anatomical targeting, treatment monitoring and control. To date, only a very small proportion of the total potential of FUS technology has been explored in clinical practice, and it is therefore expected to have a huge impact on patient care in the future. The ultrasound phased array technology reviewed here will enable optimal control and monitoring of the deposited energy with high spatial and temporal resolution. In addition, this technology may provide a way to manufacture clinical devices at reduced costs and, as a result, help expand the availability of such high-end medical care to low-income countries.

## Acknowledgements

The authors would like to thank the anonymous reviewers for their helpful suggestions, which have positively shaped the manuscript. Support for this work was provided by a grant (R01 EB003268) from the National Institute of Biomedical Imaging and Bioengineering of the National Institutes of Health (KH), two operating grants (MOP 119312 and MOP 142181) from the Canadian Institutes of Health Research (KH), the W. Garfield Weston Foundation, the Canada Research Chair program (KH), a Walter C. Sumner Memorial Fellowship (RMJ), and a Natural Sciences and Engineering Research Council of Canada Alexander Graham Bell Canada Graduate Scholarship (RMJ).

## References

[1]. Gawande A. Two hundred years of surgery. N. Engl. J. Med. 2012; 366:1716–23. [PubMed: 22551130]

[2]. Lynn JG, Zwemer RL, Chick AJ, Miller AE. A new method for the genereation and use of focused ultrasound in experimental biology. J. Gen. Physiol. 1942; 26:179–93. [PubMed: 19873337]

[3]. Lynn JG, Putnam TJ. Histology of cerebral lesions produced by focused ultrasound. Am. J. Pathol. 1944; 20:637–49. [PubMed: 19970769]

[4]. Fry WJ. Use of intense ultrasound in neurological research. Am. J. Phys. Med. 1958; 37:143–7. [PubMed: 13545380]

[5]. Fry WJ, Fry FJ. Fundamental neurological research and human neurosurgery using intense ultrasound. IRE Trans. Med. Electron. 1960; ME-7:166–81. [PubMed: 13702332]

[6]. Fry FJ, Sanghvi NT, Eggleton RC, Erdmann W. Ultrasonic visualization and therapeutic computer controlled system. Ultrasound in Medicine. 1976; 2:481–2.

[7]. Vallancien G, Harouni M, Veillon B, Mombet A, Prapotnich D, Brisset JM, Bougaran J. Focused extracorporeal pyrotherapy: feasibility study in man. J. Endourol. 1992; 6:173–81.

[8]. Wu F, Chen W-Z, Bai J, Zou J-Z, Wang Z-L, Zhu H, Wang Z-B. Pathological changes in human malignant carcinoma treated with high-intensity focused ultrasound. Ultrasound Med. Biol. 2001; 27:1099–1106. [PubMed: 11527596]

[9]. Warmuth M, Johansson T, Mad P. Systematic review of the efficacy and safety of high-intensity focussed ultrasound for the primary and salvage treatment of prostate cancer. Eur. Urol. 2010; 58:803–15. [PubMed: 20864250]

[10]. Hynynen K, Darkazanli A, Unger E, Schenck JF. MRI-guided noninvasive ultrasound surgery. Med. Phys. 1993; 20:107–115. [PubMed: 8455489]

[11]. Catane R, et al. MR-guided focused ultrasound surgery (MRgFUS) for the palliation of pain in patients with bone metastases–preliminary clinical experience. Ann. Oncol. 2007; 18:163–7. [PubMed: 17030549]

[12]. Hynynen K. MRIgHIFU: A tool for image-guided therapeutics. J. Magn. Reson. Imaging. 2011; 34:482–93. [PubMed: 22896850]

[13]. Uchida T, Tomonaga T, Kim H, Nakano M, Shoji S, Najata Y, Terachi T. Improved outcomes with advancements in high intensity focused ultrasound devices for the treatment of localized prostate cancer. J. Urol. 2015; 193:103–10. [PubMed: 25079940]

[14]. Foster RS, Bihrle R, Sanghvi NT, Donohue JP, Fry FJ. High intensity focused ultrasound treatment of human BPH. Prog. Clin. Biol. Res. 1994; 386:463–71. [PubMed: 7528416]

[15]. Gelet A, Chapelon JY, Bouvier R, Souchon R, Pangaud C, Abdelrahim AF, Cathignol D, Dubernard JM. Treatment of prostate cancer with transrectal focused ultrasound: early clinical experience. Eur. Urol. 1995; 29:174–83. [PubMed: 8647143]

[16]. Huber PE, Jenne JW, Rastert R, Simiantonakis I, Sinn H-P, Strittmatter H-J, von Fournier D, Wannenmacher MF, Debus J. A new noninvasive approach in breast cancer therapy using magnetic resonance imaging-guided focused ultrasound surgery. Cancer Res. 2001; 61:8441–7. [PubMed: 11731425]

[17]. Hynynen K, Pomeroy O, Smith DN, Huber PE, McDannold NJ, Kettenbach J, Baum J, Singer S, Jolesz FA. MR imaging-guided focused ultrasound surgery of fibroadenomas in the breast: a feasibility study. Radiology. 2001; 219:176–85. [PubMed: 11274554]

[18]. Tempany CMC, Stewart EA, McDannold N, Quade BJ, Jolesz FA, Hynynen K. MR imaging-guided focused ultrasound surgery of uterine leiomyomas: a feasibility study. Radiology. 2003; 226:897–905. [PubMed: 12616023]

[19]. Ocheltree KB, Benkeser PJ, Frizzell LA, Cain CA. An ultrasonic phased array applicator for hyperthermia. IEEE Trans. Sonics Ultrason. 1984; 31:526–31.

[20]. Cain CA, Umemura S-I. Concentric-ring and sector-vortex phased-array applicators for ultrasound hyperthermia. IEEE Trans. Microw. Theory Techn. 1986; 34:542–51.

[21]. Fan X, Hynynen K. A study of various parameters of spherically curved phased arrays for noninvasive ultrasound surgery. Phys. Med. Biol. 1996; 41:591–608. [PubMed: 8730659]

[22]. Fjield T, Hynynen K. Experimental verification of the sectored annular phased array for MRI guided ultrasound surgery. Proc. IEEE Ultrason. Symp. 1996:1273–6.

[23]. Hynynen K, Clement G. Clinical applications of focused ultrasound–the brain. Int. J. Hyperthermia. 2007; 23:193–202. [PubMed: 17578343]

[24]. Somer JC. Electronic sector scanning for ultrasonic diagnosis. Ultrasonics. 1968; 6:153–9. [PubMed: 5716157]

[25]. Wells, PNT. Biomedical Ultrasonics. Academic Press; London: 1977.

[26]. Cobbold, RSC. Foundations of Biomedical Ultrasound. Oxford University Press; Oxford: 2007.

[27]. Newnham RE, Bowen LJ, Klicker KA, Cross LE. Composite piezoelectric transducers. Mater. Des. 1980; 2:93–106.

[28]. Chapelon J-Y, Cathignol D, Cain C, Ebbini E, Kluiwstra J-U, Sapozhnikov OA, Fleury G, Berriet R, Chupin L, Guey J-L. New piezoelectric transducers for therapeutic ultrasound. Ultrasound Med. Biol. 2000; 26:153–9. [PubMed: 10687803]

[29]. Daum DR, Hynynen K. A 256-element ultrasonic phased array system for the treatment of large volumes of deep seated tissue. IEEE Trans. Ultrason. Ferroelectr. Freq. Control. 1999; 46:1254–68. [PubMed: 18244318]

[30]. Wells PNT. Absorption and dispersion of ultrasound in biological tissue. Ultrasound Med. Biol. 1975; 1:369–76. [PubMed: 1098249]

[31]. O'Neil HT. Theory of focusing radiators. J. Acoust. Soc. Am. 1949; 21:516–26.

[32]. Beard RE, Magin RL, Frizzell LA, Cain CA. An annular focus ultrasonic lens for local hyperthermia treatment of small tumors. Ultrasound Med. Biol. 1982; 8:177–84. [PubMed: 7071993]

[33]. Fjield T, Sorrentino V, Cline H, Hynynen K. Design and experimental verification of thin acoustic lenses for the coagulation of large tissue volumes. Phys. Med. Biol. 1997; 42:2341–54. [PubMed: 9434292]

[34]. Meininger, et al. Initial experience with a novel focused ultrasound ablation system for ring ablation outside the pulmonary vein. J. Interv. Card. Electrophysiol. 2003; 8:141–8. [PubMed: 12766506]

[35]. Baker KG, Robertson VJ, Duck FA. A review of therapeutic ultrasound: biophysical effects. Phys. Ther. 2001; 81:1351–8. [PubMed: 11444998]

[36]. O'Brien WD. Ultrasound-biophysics mechanisms. Prog. Biophys. Mol. Biol. 2007; 93:212–55. [PubMed: 16934858]

[37]. ter Haar G, Coussios C. High intensity focused ultrasound: physical principles and devices. Int. J. Hyperthermia. 2007; 23:89–104. [PubMed: 17578335]

[38]. Song CW. Effect of local hyperthermia on blood flow and microenvironment: a review. Cancer Res. 1984; 44:4721–30.

[39]. Goldberg SN, Gazelle GS, Mueller PR. Thermal ablation therapy for focal malignancy: a unified approach to underlying principles, techniques, and diagnostic imaging guidance. Am. J. Roentgenol. 2000; 174:323–31. [PubMed: 10658699]

[40]. Leighton, TG. The Acoustic Bubble. Academic Press; San Diego: 1994.

[41]. Maxwell AD, Wang T-Y, Cain CA, Fowlkes JB, Sapozhnikov OA, Bailey MR, Xu Z. Cavitation clouds created by shock scattering from bubbles during histotripsy. J. Acoust. Soc. Am. 2011; 130:1888–98. [PubMed: 21973343]

[42]. Lin K-W, Hall TL, McGough RJ, Xu Z, Cain CA. Synthesis of monopolar ultrasound pulses for therapy: the frequency-compounding transducer. IEEE Trans. Ultrason. Ferroelectr. Freq. Control. 2014; 61:1123–36. [PubMed: 24960702]

[43]. Khokhlova TD, Canney MS, Khokhlova VA, Sapozhnikov OA, Crum LA, Bailey MR. Controlled tissue emulsification produced by high intensity focused ultrasound shock waves and millisecond boiling. J. Acoust. Soc Am. 2011; 130:3498–510. [PubMed: 22088025]

[44]. Wang Y-N, Khokhlova T, Bailey M, Hwang JH, Khokhlova V. Histological and biochemical analysis of mechanical and thermal bioeffects in boiling histotripsy lesions induced by high intensity focused ultrasound. Ultrasound Med. Biol. 2013; 39:424–38. [PubMed: 23312958]

[45]. Chatelin S, Gennisson J-L, Bernal M, Tanter M, Pernot M. Modelling the impulse diffraction field of shear waves in transverse isotropic viscoelastic medium. Phys. Med. Biol. 2015; 60:3639–54. [PubMed: 25880794]

[46]. Hynynen K, McDannold N, Vykhodtseva N, Jolesz FA. Noninvasive MR imaging-guided focal opening of the blood-brain barrier in rabbits. Radiology. 2001; 220:640–6. [PubMed: 11526261]

[47]. Tran BC, Seo J, Hall TL, Fowlkes JB, Cain CA. Microbubble-enhanced cavitation for noninvasive ultrasound surgery. IEEE Trans. Ultrason. Ferroelectr. Freq. Control. 2003; 50:1296–1304. [PubMed: 14609069]

[48]. Kripfgans OD, Fowlkes JB, Miller DL, Eldevik OP, Carson PL. Acoustic droplet vaporization for therapeutic and diagnostic applications. Ultrasound Med. Biol. 2000; 26:1177–89. [PubMed: 11053753]

[49]. Coussios CC, Roy RA. Applications of acoustics and cavitation to noninvasive therapy and drug delivery. Annu. Rev. Fluid Mech. 2008; 40:395–420.

[50]. Lingeman JE, McAteer JA, Gnessin E, Evan AP. Shock wave lithotripsy: advances in technology and technique. Nat. Rev. Urol. 2009; 6:660–670. [PubMed: 19956196]

[51]. O'Reilly MA, Hynynen K. Ultrasound enhanced drug delivery to the brain and central nervous system. Int. J. Hyperthermia. 2012; 28:386–96. [PubMed: 22621739]

[52]. Kooiman K, Vos HJ, Versluis M, de Jong N. Acoustic behavior of microbubbles and implications for drug delivery. Adv. Drug Deliver. Rev. 2014; 72:28–48.

[53]. de Saint Victor M, Crake C, Coussios C-C, Stride E. Properties, characteristics and applications of microbubbles for sonothrombolysis. Expert Opin. Drug Deliv. 2014; 11:1–23. [PubMed: 24093806]

[54]. Khokhlova VA, Fowlkes JB, Roberts WW, Schade GR, Xu Z, Khokhlova TD, Hall TL, Maxwell AD, Wang Y-N, Cain CA. Histotripsy methods in mechanical disintegration of tissue: Towards clinical applications. Int. J. Hyperthermia. 2015; 31:145–162. [PubMed: 25707817]

[55]. Sarvazyan AP, Rudenko OV, Nyborg WL. Biomedical applications of radiation force of ultrasound: historical roots and physical basis. Ultrasound Med. Biol. 2010; 36:1379–94. [PubMed: 20800165]

[56]. Dalecki D, Keller BB, Raeman CH, Carstensen EL. Effects of pulsed ultrasound on the frog heart: I. Thresholds for changes in cardiac rhythm and aortic pressure. Ultrasound Med. Biol. 1993; 19:385–90. [PubMed: 8356782]

[57]. Acconcia C, Leung BYC, Manjunath A, Goertz DE. Interactions between individual ultrasound-stimulated microbubbles and fibrin clots. Ultrasound Med. Biol. 2014; 40:2134–50. [PubMed: 24882525]

[58]. Bader KB, Gruber MJ, Holland CK. Shaken and stirred: mechanisms of ultrasound-enhanced thrombolysis. Ultrasound Med. Biol. 2014; 41:187–96. [PubMed: 25438846]

[59]. Francis CW, Blinc A, Lee S, Cox C. Ultrasound accelerates transport of recombinant tissue plasminogen activator into clots. Ultrasound Med. Biol. 1995; 21:419–24. [PubMed: 7645133]

[60]. Shah A, Owen NR, Lu W, Cunitz BW, Kaczkowski PJ, Harper JD, Bailey MR, Crum LA. Novel ultrasound method to reposition kidney stones. Urol. Res. 2010; 38:491–5. [PubMed: 20967437]

[61]. Sorensen MD, Bailey MR, Hsi RS, Cunitz BW, Simon JC, Wang Y-N, Dunmire BL, Paun M, Starr F, Lu W, Evan AP, Harper JD. Focused ultrasonic propulsion of kidney stones: review and update of preclinical technology. Journal of Endourology. 2013; 27:1183–6. [PubMed: 23883117]

[62]. Duryea AP, Cain CA, Roberts WW, Hall TL. Removal of residual cavitation nuclei to enhance histotripsy fractionation of soft tissue. IEEE Ultrason. Ferroelectr. Freq. Control. 2015; 62:2068–78.

[63]. Stewart JL, Westerfield EC. A theory of active sonar detection. Proc. IRE. 1959; 41:872–82.

[64]. von Aulock WH. Properties of phased arrays. Proc. IRE. 1960; 41:1715–27.

[65]. Hunt JW, Arditi M, Foster FS. Ultrasound transducers for pulse-echo medical imaging. IEEE Trans. Biomed. Eng. 1983; 30:453–481. [PubMed: 6629380]

[66]. Do-Huu JP, Hartemann P. Annular array transducer for deep acoustic hyperthermia. IEEE Symp. 1981; 41:705–10.

[67]. Duck, FA. Physical Properties of Tissue: A Comprehensive Reference Book. Academic Press; London: 1990.

[68]. Foster FS, Larson JD, Mason MK, Shoup TS, Nelson G, Yoshida H. Development of a 12 element annular array transducer for realtime ultrasound imaging. Ultrasound Med. Biol. 1989; 15:649–59. [PubMed: 2683291]

[69]. Chapelon JY, Faure P, Plantier M, Cathignol D, Souchon R, Gorry F, Gelet A. The feasibility of tissue ablation using high intensity electronically focused ultrasound. Proc. IEEE Ultrason. Symp. 1993; 41:1211–4.

[70]. Petrusca L, Ngo J, Brasset L, Blanc E, Murillo A, Auboiroux V, Cotton F, Chapelon J-Y, Salomir R. Experimental investigation of MRgHIFU sonication with interleaved electronic and mechanical displacement of the focal point for transrectal prostate application. Phys. Med. Biol. 2012; 57:4805–25. [PubMed: 22772091]

[71]. Buchanan MT, Hynynen K. Design and experimental evaluation of an intracavitary ultrasound phased array system for hyperthermia. IEEE Trans. Biomed. Eng. 1994; 41:1178–87. [PubMed: 7851919]

[72]. Diederich CJ, Burdette EC. Transurethral ultrasound array for prostate thermal therapy: initial studies. IEEE Trans. Ultrason. Ferroelectr. Freq. Control. 1996; 43:1011–22.

[73]. Gavrilov LR, Hand JW. Development and investigation of ultrasound linear phased arrays for transrectal treatment of prostate. Ultrason. Sonochem. 1997; 4:173–4. [PubMed: 11237037]

[74]. Wildes DG, Chiao RY, Daft CMW, Rigby KW, Smith LS, Thomenius KE. Elevation performance of 1.25 D and 1.5 D transducer arrays. IEEE Ultrason. Ferroelectr. Freq. Control. 1997; 44:1027–37.

[75]. Curiel L, Chavrier F, Souchon R, Birer A, Chapelon JY. 1.5-D high intensity focused ultrasound array for non-invasive prostate cancer surgery. IEEE Ultrason. Ferroelectr. Freq. Control. 2002; 49:231–42.

[76]. Saleh KY, Smith NB. A 63 element 1.75 dimensional ultrasound phased array for the treatment of benign prostatic hyperplasia. Biomed. Eng. Onine. 2005; 4:1–14.

[77]. Ebbini ES, Cain CA. Multiple-focus ultrasound phased-array pattern synthesis: optimal driving-signal distributions for hyperthermia. IEEE Ultrason. Ferroelectr. Freq. Control. 1989; 36:540–8.

[78]. Ebbini ES, Cain CA. Experimental evaluation of a prototype cylindrical section ultrasound hyperthermia phased-array applicator. IEEE Ultrason. Ferroelectr. Freq. Control. 1991; 38:510–20.

[79]. Fjield T, Hynynen K. The combined concentric-ring and sector-vortex phased array for MRI guided ultrasound surgery. IEEE Ultrason. Ferroelectr. Freq. Control. 1997; 44:1157–67.

[80]. Daum DR, Buchanan MT, Fjield T, Hynynen K. Design and evaluation of a feedback based phased array system for ultrasound surgery. IEEE Ultrason. Ferroelectr. Freq. Control. 1998; 45:431–8.

[81]. Daum, Hynynen K. Thermal dose optimization via temporal switching in ultrasound surgery. IEEE Ultrason. Ferroelectr. Freq. Control. 1998; 45:208–15.

[82]. King DD, Packard RF, Thomas RK. Unequally-spaced, broad-band antenna arrays. IRE Trans. Antennas Prop. 1960; X:380–4.

[83]. Lo YT. A mathematical theory of antenna arrays with randomly spaced elements. IRE Trans. Antennas Prop. 1964; 12:257–68.

[84]. Steinberg BD. Comparison between the peak sidelobe of the random array and algorithmically designed aperiodic arrays. IRE Trans. Antennas Prop. 1973; 21:366–70.

[85]. Turnbull DH, Foster FS. Beam steering with pulsed two-dimensional transducer arrays. IEEE Trans. Ultrason. Ferroelectr. Freq. Control. 1991; 38:320–33. [PubMed: 18267591]

[86]. Davidsen RE, Jensen JA, Smith SW. Two-dimensional random arrays for real time volumetric imaging. Ultrason. Imag. 1994; 16:143–63.

[87]. Nikolov SI, Jensen JA. Application of different spatial sampling patterns for sparse array transducer design. Ultrasonics. 2000; 37:667–71. [PubMed: 10950348]

[88]. Goss SA, Frizzell LA, Kouzmanoff JT, Barich JM, Yang JM. Sparse random ultrasound phased array for focal surgery. IEEE Trans. Ultrason. Ferroelectr. Freq. Control. 1996; 43:1111–21.

[89]. Pernot M, Aubry J-F, Tanter M, Thomas J-L, Fink M. High power transcranial beam steering for ultrasonic brain therapy. Phys. Med. Biol. 2003; 48:2577–89. [PubMed: 12974575]

[90]. Hand JW, Shaw A, Sadhoo N, Rajagopal S, Dickinson RJ, Gavrilov LR. A random phased array device for delivery of high intensity focused ultrasound. Phys. Med. Biol. 2009; 54:5675–93. [PubMed: 19724099]

[91]. Hutchinson EB, Buchanan MT, Hynynen K. Design and optimization of an aperiodic ultrasound phased array for intracavitary prostate thermal therapies. Med. Phys. 1996; 23:767–76. [PubMed: 8724752]

[92]. Pajek D, Hynynen K. The design of a focused ultrasound transducer array for the treatment of stroke: a simulation study. Phys. Med. Biol. 2012; 57:4951–68. [PubMed: 22800986]

[93]. Gu J, Jing J. Modeling of wave propagation for medical ultrasound: a review. IEEE Ultrason. Ferroelectr. Freq. Control. 2015; 62:1979–93.

[94]. D'jin WA, Burtnyk M, Bronskill M, Chopra R. Investigation of power and frequency for 3D conformal MRI-controlled transurethral ultrasound therapy with a dual frequency multi-element transducer. Int. J. Hyperthermia. 2012; 28:87–104. [PubMed: 22235788]

[95]. Ellens N, Hynynen K. Frequency considerations for deep ablation with high-intensity focused ultrasound: a simulation study. Med. Phys. 2015; 42:4896–910. [PubMed: 26233216]

[96]. Ellens N, Pulkkinen A, Song J, Hynynen K. The utility of sparse 2D fully electronically steerable focused ultrasound phased arrays for thermal surgery: a simulation study. Phys. Med. Biol. 2011; 56:4913–4932. [PubMed: 21772081]

[97]. Payne A, Vyas U, Todd N, de Bever J, Christensen DA, Parker DL. The effect of electronically steering a phased array ultrasound transducer on near-field tissue heating. Med. Phys. 2011; 38:4971–81. [PubMed: 21978041]

[98]. Pajek D, Hynynen K. The application of sparse arrays in high frequency transcranial focused ultrasound therapy: A simulation study. Med. Phys. 2013; 40:122901. 1-10. [PubMed: 24320540]

[99]. Coviello CM, Kozick RJ, Hurrell A, Smith PP, Coussio C-C. Thin-film sparse boundary array design for passive acoustic mapping during ultrasound therapy. IEEE Trans. Ultrason. Ferroeletrc. Freq. Control. 2012; 59:2322–2330.

[100]. Jones RM, O'Reilly MA, Hynynen K. Transcranial passive acoustic mapping with hemispherical sparse arrays using CT-based skull-specific aberration corrections: a simulation study. Phys. Med. Biol. 2013; 58:4981–5005. [PubMed: 23807573]

[101]. O'Reilly MA, Jones RM, Hynynen K. Three-dimensional transcranial ultrasound imaging of microbubble clouds using a sparse hemispherical array. IEEE Trans. Biomed. Eng. 2014; 61:1285–1294. [PubMed: 24658252]

[102]. Wang H, Ebbini E, Cain CA. Effect of phase errors on field patterns generated by an ultrasound phased-array hyperthermia applicator. IEEE Trans. Ultrason. Ferroeletrc. Freq. Control. 1991; 38:521–531.

[103]. Fjield T, Silcox CE, Hynynen K. Low-profile lenses for ultrasound surgery. Phys. Med. Biol. 1999; 44:1803–13. [PubMed: 10442714]

[104]. Caulfield RE, Yin X, Juste J, Hynynen K. A novel phase assignment protocol and driving system for a high-density focused ultrasound array. IEEE Trans. Ultrason. Ferroeletrc. Freq. Control. 2007; 54:793–801.

[105]. Park SB, Kwak J, Lee K. An ASIC design for versatile receive front-end electronics of an ultrasonic medical imaging system–16 channel analog inputs and 4 dynamically focused beam outputs. Ultrason. Imag. 2003; 25:85–108.

[106]. Hynynen K, Yin J. Lateral mode coupling to reduce the electrical impedance of small elements required for high power ultrasound therapy phased arrays. IEEE Trans. Ultrason. Ferroeletrc. Freq. Control. 2009; 56:557–564.

[107]. Song J, Hynynen K. Feasibility of using lateral mode coupling method for a large scale ultrasound phased array for noninvasive transcranial therapy. IEEE Trans. Biomed. Eng. 2010; 57:124–33. [PubMed: 19695987]

[108]. Song J, Lucht B, Hynynen K. Large improvement of the electrical impedance of imaging and high-intensity focused ultrasound (HIFU) phased arrays using multilayer piezoelectric ceramics coupled in lateral mode. IEEE Trans. Ultrason. Ferroeletrc. Freq. Control. 2012; 59:1584–95.

[109]. Ellens NPK, Lucht BBC, Gunaseelan ST, Hudson JM, Hynynen K. A novel, flat, electronically-steered phased array transducer for tissue ablation: preliminary results. Phys. Med. Biol. 2015; 60:2195–2215. [PubMed: 25683789]

[110]. Ergun AS, Yaralioglu GG, Khuri-Yakub BT. Capacitive micromachined ultrasonic transducers: theory and technology. J. Aerosp. Eng. 2003; 16:76–84.

[111]. Jin X, Oralkan O, Degertekin FL, Khuri-Yakub BT. Characterization of one-dimensional capacitive micromachined ultrasonic immersion transducer arrays. IEEE Trans. Ultrason. Ferroeletrc. Freq. Control. 2001; 48:750–60.

[112]. Christiansen TL, Rasmussen MF, Bagge JP, Moesner LN, Jensen JA, Thomsen EV. 3-D imaging using row–column-addressed arrays with integrated apodization–part ii: transducer fabrication and experimental results. IEEE Trans. Ultrason. Ferroeletrc. Freq. Control. 2015; 62:959–71.

[113]. Wong SH, Kupnik M, Watkins RD, Butts-Pauly K, Khuri-Yakub BT. Capacitive micromachined ultrasonic transducers for therapeutic ultrasound applications. IEEE Trans. Biomed. Eng. 2010; 57:114–23. [PubMed: 19628448]

[114]. Civale C, Rivens I, ter Haar G. Quality assurance for clinical high intensity focused ultrasound fields. Int. J. Hyperthermia. 2015; 31:193–202. [PubMed: 25677839]

[115]. Schafer ME, Lewin PA. Transducer characterization using the angular spectrum method. J. Acoust. Soc. Am. 1989; 85:2202–14.

[116]. Clement GT, Hynynen K. Field characterization of therapeutic ultrasound phased arrays through forward and backward planar projection. J. Acoust. Soc. Am. 2010; 108:441–6. [PubMed: 10923906]

[117]. Kreider W, Yuldashev PV, Sapozhnikov OA, Farr N, Partanen A, Bailey MR, Khokhlova VA. Characterization of a multi-element clinical HIFU system using acoustic holography and nonlinear modeling. IEEE Trans. Ultrason. Ferroeletrc. Freq. Control. 60:1683–98.

[118]. Sapozhnikov OA, Tsysar SA, Khokhlova VA, Kreider W. Acoustic holography as a metrological tool for characterizing medical ultrasound sources and fields. J. Acoust. Soc. Am. 2015; 138:1515–32. [PubMed: 26428789]

[119]. Fan X, Hynynen K. Ultrasound surgery using multiple sonications–treatment time considerations. Ultrasound Med. Biol. 1996; 22:471–82. [PubMed: 8795174]

[120]. Wan H, VanBaren P, Ebbini ES, Cain CA. Ultrasound surgery: comparison of strategies using phased array systems. IEEE Trans. Ultrason. Ferroeletrc. Freq. Control. 1996; 43:1085–98.

[121]. Lele PP. Induction of deep, local hyperthermia by ultrasound and electromagnetic fields: problems and choices. Radiat. Environ. Biophys. 1980; 17:205–17. [PubMed: 7443976]

[122]. Moros EG, Roemer RB, Hynynen K. Simulations of scanned focused ultrasound hyperthermia: the effects of scanning speed and pattern on the temperature fluctuations at the focal depth. IEEE Trans. Ultrason. Ferroeletrc. Freq. Control. 1988; 35:552–60.

[123]. Rieke V, Instrella R, Rosenberg J, Grissom W, Werner B, Martin E, Butts-Pauly K. Comparison of temperature processing methods for monitoring focused ultrasound ablation in the brain. J. Magn. Reson. Imaging. 2013; 38:1462–71. [PubMed: 23559437]

[124]. Goertz DE, Wright C, Hynynen K. Contrast agent kinetics in the rabbit brain during exposure to therapeutic ultrasound. Ultrasound Med. Biol. 2010; 36:916–24. [PubMed: 20447757]

[125]. Smith NB, Hynynen K. The feasibility of using focused ultrasound for transmyocardial revascularization. Ultrasound Med. Biol. 1998; 24:1045–54. [PubMed: 9809638]

[126]. Phillips DJ, Smith SW, von Ramm OT, Thurstone FL. Sampled aperture techniques applied to B-mode echoencephalography. Acoust. Hologr. 1975; 6:103–120.

[127]. Thomas JL, Fink MA. Ultrasonic beam focusing through tissue inhomogeneities with a time reversal mirror: application to transskull therapy. IEEE Trans. Ultrason. Ferroelectr. Freq. Control. 1996; 43:1122–9.

[128]. Hynynen K, Jolesz FA. Demonstration of potential noninvasive ultrasound brain therapy through an intact skull. Ultrasound Med. Biol. 1998; 24:27583.

[129]. White J, Clement GT, Hynynen K. Transcranial ultrasound focus reconstruction with phase and amplitude correction. IEEE Trans. Ultrason. Ferroelectr. Freq. Control. 2005; 52:1518–22. [PubMed: 16285450]

[130]. Botros YY, Ebbini ES, Volakis JL. Two-step hybrid virtual array ray (VAR) technique for focusing through the rib cage. IEEE Trans. Ultrason. Ferroelectr. Freq. Control. 1998; 45:989–1000. [PubMed: 18244253]

[131]. Aubry J-F, Pernot M, Marquet F, Tanter M, Fink M. Transcostal high-intensity-focused ultrasound: ex vivo adaptive focusing feasibility study. Phys. Med. Biol. 2008; 53:2937–51. [PubMed: 18475006]

[132]. Bobkova S, Gavrilov L, Khokhlova V, Shaw A, Hand J. Focusing of high-intensity ultrasound through the rib cage using a therapeutic random phased array. Ultrasound Med. Biol. 2010; 36:888–906. [PubMed: 20510186]

[133]. Clement GT, Hynynen K. Micro-receiver guided transcranial beam steering. IEEE Trans. Ultrason. Ferroelectr. Freq. Control. 2002; 49:44753.

[134]. Pernot M, Montaldo G, Tanter M, Fink M. "Ultrasonic stars" for time-reversal focusing using induced cavitation bubbles. Appl. Phys. Lett. 2006; 88:034102. 3pp.

[135]. Haworth KJ, Fowlkes JB, Carson PL, Kripfgans OD. Towards aberration correction of transcranial ultrasound using acoustic droplet vaporization. Ultrasound Med. Biol. 2008; 34:435–45. [PubMed: 17935872]

[136]. Gateau J, Marsac L, Pernot M, Aubry JF, Tanter M, Fink M. Transcranial ultrasonic therapy based on time reversal of acoustically induced cavitation bubble signature. IEEE Trans. Biomed. Eng. 2010; 57:134–44. [PubMed: 19770084]

[137]. OReilly MA, Hynynen K. A super-resolution ultrasound method for brain vascular mapping. Med. Phys. 2013; 40:110701. 7pp. [PubMed: 24320408]

[138]. Vignon F, Aubry JF, Tanter M, Margoum A, Fink M. Adaptive focusing for transcranial ultrasound imaging using dual arrays. J. Acoust. Soc. Am. 2006; 120:2737–45. [PubMed: 17139734]

[139]. Aarnio J, Clement GT, Hynynen K. A new ultrasound method for determining the acoustic phase shifts caused by the skull bone. Ultrasound Med. Biol. 2005; 31:771–80. [PubMed: 15936493]

[140]. Hertzberg Y, Volovick A, Zur Y, Medan Y, Vitek S, Navon G. Ultrasound focusing using magnetic resonance acoustic radiation force imaging: application to ultrasound transcranial therapy. Med. Phys. 2010; 37:2934–42. [PubMed: 20632605]

[141]. Hynynen K, Sun J. Trans-skull ultrasound therapy: the feasibility of using image-derived skull thickness information to correct the phase distortion. IEEE Trans. Ultrason. Ferroelectr. Freq. Control. 1999; 46:752–5. [PubMed: 18238476]

[142]. Wintermark M, et al. T1-weighted MRI as a substitute to CT for refocusing planning in MR-guided focused ultrasound. Phys. Med. Biol. 2014; 59:3599–614. [PubMed: 24909357]

[143]. Miller GW, Eames M, Snell J, Aubry JF. Ultrashort echo-time MRI versus CT for skull aberration correction in MR-guided transcranial focused ultrasound: in vitro comparison on human calvaria. Med. Phys. 2015; 42:2223–33. [PubMed: 25979016]

[144]. Clement GT, Hynynen K. A non-invasive method for focusing ultrasound through the human skull. Phys. Med. Biol. 2002; 47:1219–36. [PubMed: 12030552]

[145]. Aubry JF, Tanter M, Pernot M, Thomas JL, Fink M. Experimental demonstration of noninvasive transskull adaptive focusing based on prior computed tomography scans. J. Acoust. Soc. Am. 2003; 113:84–93. [PubMed: 12558249]

[146]. Jones RM, Hynynen K. Comparison of analytical and numerical approaches for CT-based aberration correction in transcranial passive acoustic imaging. Phys. Med. Biol. 2016; 61:23–36. [PubMed: 26605827]

[147]. Ballard JR, Casper AJ, Wan Y, Ebbini ES. Adaptive transthoracic refocusing of dual-mode ultrasound arrays. IEEE Trans. Biomed. Eng. 2010; 57:93–102. [PubMed: 19651547]

[148]. Quesson B, Merle M, Kohler MO, Mougenot C, Roujol S, Denis de Senneville B, Moonen CT. A method for MRI guidance of intercostal high intensity focused ultrasound ablation in the liver. Med. Phys. 2010; 37:2533–40. [PubMed: 20632565]

[149]. Cain CA, Umemura S-I. Annular and sector phased array applicators for ultrasound hyperthermia. Proc. IEEE Ultrason. Symp. 1985:936–41.

[150]. Ebbini ES, Ibbini MS, Cain CA. An inverse method for hyperthermia phased-array pattern synthesis. Proc. IEEE Ultrason. Symp. 1988:947–50.

[151]. Ibbini MS, Cain CA. A field conjugation method for direct synthesis of hyperthermia phased-array heating patterns. IEEE Trans. Ultrason. Ferroeletrc. Freq. Control. 1989; 36:3–9.

[152]. Ebbini ES, Cain CA. Optimization of the intensity gain of multiple-focus phased-array heating patterns. Int. J. Hyperthermia. 1991; 7:953–73. [PubMed: 1806647]

[153]. McGough RJ, Ebbini ES, Cain CA. Direct computation of ultrasound phased-array driving signals from a specified temperature distribution for hyperthermia. IEEE Trans. Biomed. Eng. 39:825–35. [PubMed: 1505996]

[154]. Partanen A, Tillander M, Yarmolenko PS, Wood BJ, Dreher MR, Kohler MO. Reduction of peak acoustic pressure and shaping of heated region by use of multifoci sonications in MR-guided high-intensity focused ultrasound mediated mild hyperthermia. Med. Phys. 2013; 40:013301. 13pp. [PubMed: 23298120]

[155]. Fan X, Hynynen K. Control of the necrosed tissue volume during noninvasive ultrasound surgery using a 16-element phased array. Med. Phys. 1995; 22:297–306. [PubMed: 7596319]

[156]. Hertzberg Y, Naor O, Volovick A, Shoham S. Towards multifocal ultrasonic neural stimulation: pattern generation algorithms. J. Neural Eng. 2010; 7:056002. 9pp. [PubMed: 20720281]

[157]. Seo J, Lee J. Anti-foci for focused ultrasound. Int. J. Hyperthermia. 2009; 25:566–80. [PubMed: 19848619]

[158]. Pulkkinen A, Huang Y, Song J, Hynynen K. Simulations and measurements of transcranial low-frequency ultrasound therapy: skull-base heating and effective area of treatment. Phys. Med. Biol. 2011; 56:4661–83. [PubMed: 21734333]

[159]. Vaezy S, Andrew M, Kaczkowski P, Crum L. Image-guided acoustic therapy. Ann. Rev. Biomed. Eng. 2001; 3:375–90. [PubMed: 11447068]

[160]. Ebbini ES, ter Haar G. Ultrasound-guided therapeutic focused ultrasound: Current status and future directions. Int. J. Hyperthermia. 2015; 31:77–89. [PubMed: 25614047]

[161]. McDannold N. Quantitative MRI-based temperature mapping based on the proton resonant frequency shift: review of validation studies. Int. J. Hyperthermia. 2005; 21:533–46. [PubMed: 16147438]

[162]. Rieke V, Pauly KB. MR thermometry. J. Magn. Reson. Imaging. 2008; 27:376–90. [PubMed: 18219673]

[163]. Hynynen K, Vykhodtseva NI, Chung AH, Sorrentino V, Colluci V, Jolesz FA. Thermal effects of focused ultrasound on the brain: determination with MR imaging. Radiology. 1997; 204:247–53. [PubMed: 9205255]

[164]. Ishihara Y, Calderon A, Watanabe H, Okamoto K, Suzuki Y, Kuroda K, Suzuki Y. A precise and fast temperature mapping using water proton chemical shift. Magn. Reson. Med. 1995; 34:814–23. [PubMed: 8598808]

[165]. De Poorter J, De Wagter C, De Deene Y, Thomsen C, Stahlberg F, Achten E. Noninvasive MRI thermometry with the proton resonance frequency (PRF) method: *in vivo* results in human muscle. Magn. Reson. Med. 1995; 33:74–81. [PubMed: 7891538]

[166]. Kuroda K, Oshio K, Mulkern RV, Jolesz FA. Optimization of chemical shift selective suppression of fat. Magn. Reson Med. 1998; 40:505–10. [PubMed: 9771566]

[167]. de Zwart JA, Vimeux FC, Delalande C, Canioni P, Moonen CTW. Fast lipid-suppressed MR temperature mapping with echo-shifted gradient-echo imaging and spectral-spatial excitation. Magn. Reson. Med. 1998; 42:53–9. [PubMed: 10398950]

[168]. Kaye EA, Chen J, Pauly KB. Rapid MR-ARFI method for focal spot localization during focused ultrasound therapy. Magn. Reson Med. 2011; 65:738–43. [PubMed: 21337406]

[169]. Chung AH, Jolesz FA, Hynynen K. Thermal dosimetry of a focused ultrasound beam in vivo by magnetic resonance imaging. Med. Phys. 1999; 26:2017–26. [PubMed: 10505893]

[170]. Sapareto SA, Dewey WC. Thermal dose determination in cancer therapy. Int. J. Radiat. Oncol. Biol. Phys. 1984; 10:787–800. [PubMed: 6547421]

[171]. Hutchinson E, Dahleh M, Hynynen K. The feasibility of MRI feedback control for intracavitary phased array hyperthermia treatments. Int. J. Hyperthermia. 1998; 14:39–56. [PubMed: 9483445]

[172]. Vimeux FC, De Zwart JA, Palussiere J, Fawaz R, Delalande C, Canioni P, Grenier N, Moonen CT. Real-time control of focused ultrasound heating based on rapid MR thermometry. Invest. Radiol. 1999; 34:190–3. [PubMed: 10084662]

[173]. Chopra R, Burtnyk M, N-djin WA, Bronskill M. MRI-controlled transurethral ultrasound therapy for localised prostate cancer. Int. J. Hyperthermia. 2010; 26:804–21. [PubMed: 21043572]

[174]. Enholm JK, Kohler MO, Quesson B, Mougenot C, Moonen CTW, Sokka SD. Improved volumetric MR-HIFU ablation by robust binary feedback control. IEEE Trans. Biomed. Eng. 2010; 45:103–13. [PubMed: 19846364]

[175]. Hynynen K, Darkazanli A, Damianou CA, Unger E, Schenck JF. The usefulness of a contrast agent and gradient-recalled acquisition in a steady-state imaging sequence for magnetic resonance imaging-guided noninvasive ultrasound surgery. Invest. Radiol. 1994; 29:897–903. [PubMed: 7852041]

[176]. Wu T, Felmlee JP, Greenleaf JF, Riederer SJ, Ehman RL. Assessment of thermal tissue ablation with MR elastography. Magn. Reson. Med. 2001; 45:80–7. [PubMed: 11146489]

[177]. Pilatou MC, Stewart EA, Maier SE, Fennessy FM, Hynynen K, Tempany CMC, McDannold N. MRI-based thermal dosimetry and diffusion-weighted imaging of MRI-guided focused ultrasound thermal ablation of uterine fibroids. J. Magn. Reson. Imaging. 2009; 29:404–11. [PubMed: 19161196]

[178]. Morocz IA, Hynynen K, Gudbjartsson H, Peled S, Colucci V, Jolesz FA. Brain edema development after MRI-guided focused ultrasound treatment. J. Magn. Reson. Imaging. 1998; 8:136–42. [PubMed: 9500273]

[179]. Chen L, Bouley D, Yuh E, D'Arceuil, Butts K. Study of focused ultrasound tissue damage using MRI and histology. J. Magn. Reson. Imaging. 1999; 10:146–53. [PubMed: 10441017]

[180]. Liu H-L, Wai Y-Y, Chen W-S, Chen J-C, Hsu P-H, Wu X-Y, Huang W-C, Yen T-C, Wang J-J. Hemorrhage detection during focused-ultrasound induced blood-brain-barrier opening by using susceptibility-weighted magnetic resonance imaging. Ultrasound Med. Biol. 2008; 34:598–606. [PubMed: 18313204]

[181]. Jeanmonod D, Werner B, Model A, Michels L, Zadicario E, Schiff G, Martin E. Transcranial magnetic resonance imaging-guided focused ultrasound: noninvasive central lateral thalamotomy for chronic neuropathic pain. Neurosurg. Focus. 2012; 32:E1. 11pp. [PubMed: 22208894]

[182]. Hynynen K, Chung AH, Colucci V, Jolesz FA. Potential adverse effects of high-intensity focused ultrasound exposure on blood vessels *in vivo*. Ultrasound Med. Biol. 1996; 22:193–201. [PubMed: 8735529]

[183]. Lewis MA, Staruch RM, Chopra R. Thermometry and ablation monitoring with ultrasound. Int. J. Hyperthermia. 2015; 31:163–81. [PubMed: 25753369]

[184]. Vaezy S, Shi X, Martin RW, Chi E, Nelson PI, Bailey MR, Crum LA. Real-time visualization of high-intensity focused ultrasound treatment using ultrasound imaging. Ultrasound Med. Biol. 2001; 27:33–42. [PubMed: 11295268]

[185]. Lizzi FL, Muratore R, Deng CX, Ketterling JA, Alam SK, Mikaelian S, Kalisz A. Radiation-force technique to monitor lesions during ultrasonic therapy. Ultrasound Med. Biol. 2003; 29:1593–1605. [PubMed: 14654155]

[186]. Souchon R, Rouviere O, Gelet A, Detti V, Srinivasan S, Ophir J, Chapelon J-Y. Visualisation of HIFU lesions using elastography of the human prostate *in vivo*: preliminary results. Ultrasound Med. Biol. 2003; 29:1007–15. [PubMed: 12878247]

[187]. Bercoff J, Pernot M, Tanter M, Fink M. Monitoring thermally-induced lesions with supersonic shear imaging. Ultrason. Imag. 2004; 26:74–81.

[188]. Maleke C, Konofagou EE. Harmonic motion imaging for focused ultrasound (HMIFU): a fully integrated technique for sonication and monitoring of thermal ablation in tissues. Phys. Med. Biol. 2008; 53:1773–93. [PubMed: 18367802]

[189]. Curiel L, Huang Y, Vykhodtseva N, Hynynen K. Focused ultrasound treatment of VX2 tumors controlled by local harmonic motion. Phys. Med. Biol. 2009; 54:3405–19. [PubMed: 19436103]

[190]. Kennedy JE, ter Haar GR, Wu F, Gleeson FV, Roberts ISD, Middleton MR, Cranston D. Contrast-enhanced ultrasound assessment of tissue response to high-intensity focused ultrasound. Ultrasound Med. Biol. 2004; 30:851–4. [PubMed: 15219964]

[191]. Miller MW, Everbach EC, Cox C, Knapp RR, Brayman AA, Sherman TA. A comparison of the hemolytic potential of Optison and Albunex in whole human blood *in vitro*: acoustic pressure, ultrasound frequency, donor and passive cavitation detection consideration. Ultrasound Med. Biol. 2001; 27:709–21. [PubMed: 11397535]

[192]. Xu Z, Fowlkes JB, Rothman ED, Levin AM, Cain CA. Controlled ultrasound tissue erosion: The role of dynamic interaction between insonation and microbubble activity. J. Acoust. Soc. Am. 2005; 117:424–35. [PubMed: 15704435]

[193]. Datta S, Coussios CC, McAdory LE, Tan J, Porter T, de Courten-Myers G, Holland CK. Correlation of cavitation with ultrasound enhancement of thrombolysis. Ultrasound Med. Biol. 2006; 32:1257–67. [PubMed: 16875959]

[194]. McDannold N, Vykhodtseva N, Hynynen K. Targeted disruption of the blood-brain barrier with focused ultrasound: association with cavitation activity. Phys. Med. Biol. 2006; 51:793–807. [PubMed: 16467579]

[195]. Simpson DH, Chin CT, Burns PN. Pulse inversion doppler: a new method for detecting nonlinear echoes from microbubble contrast agents. IEEE Trans. Ultrason. Ferroelectr. Freq. Control. 1999; 46:372–82. [PubMed: 18238434]

[196]. Mor-Avi V, Caiani EG, Collins KA, Korcarz CE, Bednarz JE, Lang RM. Combined assessment of myocardial perfusion and regional left ventricular function by analysis of contrast-enhanced power modulation images. Circulation. 2001; 104:352–7. [PubMed: 11457757]

[197]. Eckersley RJ, Chin TC, Burns PN. Optimising phase and amplitude modulation schemes for imaging microbubble contrast agents at low acoustic power. Ultrasound Med. Biol. 2005; 31:213–9. [PubMed: 15708461]

[198]. Sato T, Uemura K, Sasaki K. Superresolution acoustical passive imaging system using algebraic reconstruction. J. Acoust. Soc. Am. 1980; 67:1802–8.

[199]. Norton SJ, Won IJ. Time exposure acoustics. IEEE Trans. Geosci. Remote Sens. 2000; 38:1337–43.

[200]. Farny CH, Holt RG, Roy RA. Temporal and spatial detection of HIFU-induced inertial and hot-vapor cavitation with a diagnostic ultrasound system. Ultrasound Med. Biol. 2009; 35:603–15. [PubMed: 19110368]

[201]. Salgaonkar VA, Datta S, Holland CK, Mast TD. Passive cavitation imaging with ultrasound arrays. J. Acoust. Soc. Am. 2009; 126:3071–83. [PubMed: 20000921]

[202]. Gyongy M, Coussios CC. Passive spatial mapping of inertial cavitation during HIFU exposure. IEEE Trans. Biomed. Eng. 2010; 57:48–56. [PubMed: 19628450]

[203]. Vignon F, Shi WT, Powers JE, Everbach EC, Liu J, Gao S, Xie F, Porter TR. Microbubble cavitation imaging. IEEE Trans. Ultrason. Ferroelectr. Freq. Control. 2013; 60:661–70. [PubMed: 23549527]

[204]. Arvanitis CD, Livingstone MS, McDannold N. Combined ultrasound and MR imaging to guide focused ultrasound therapies in the brain. Phys. Med. Biol. 2013; 58:4749–61. [PubMed: 23788054]

[205]. Arvanitis CD, Livingstone MS, Vykhodtseva N, McDannold N. Controlled ultrasound-induced blood-brain barrier disruption using passive acoustic emissions monitoring. Public Libr. Sci. One. 2012; 7:e45783. pp.

[206]. O'Reilly MA, Hynynen K. Blood-brain barrier: real-time feedback-controlled focused ultrasound disruption by using an acoustic emissions-based controller. Radiology. 2012; 263:96–106. [PubMed: 22332065]

[207]. Siegel RJ, et al. Noninvasive, transthoracic, low-frequency ultrasound augments thrombolysis in a canine model of acute myocardial infarction. Circulation. 2000; 101:2026–9. [PubMed: 10790341]

[208]. Schmidt B, Antz M, Ernst S, Ouyang F, Falk P, Chun JKR, Kuck K-H. Pulmonary vein isolation by high-intensity focused ultrasound: first-in-man study with a steerable balloon catheter. Heart Rhythm. 2007; 4:575–84. [PubMed: 17467623]

[209]. Chaussy C, Brendel W, Schmiedt E. Extracorporeally induced destruction of kidney stones by shock waves. Radiology. 1980; 263:96–106.

[210]. McDannold N, Clement GT, Black P, Jolesz F, Hynynen K. Transcranial magnetic resonance imaging-guided focused ultrasound surgery of brain tumors: initial findings in 3 patients. Neurosurgery. 2010; 66:323–32. [PubMed: 20087132]

[211]. Jones RM, OReilly MA, Hynynen K. Experimental demonstration of passive acoustic imaging in the human skull cavity using CT-based aberration corrections. Med. Phys. 2015b; 42:4385–400. [PubMed: 26133635]

[212]. Arvanitis CD, Clement GT, McDannold N. Transcranial assessment and visualization of acoustic cavitation: modeling and experimental validation. IEEE Trans. Med. Imag. 2015; 34:1270–81.

[213]. Fallone BG, Moran PR, Podgorsak EB. Noninvasive thermometry with a clinical xray CT scanner. Med. Phys. 1982; 9:715–21. [PubMed: 7155074]

[214]. Huang Y, Curiel L, Kukic A, Plewes DB, Chopra R, Hynynen K. MR acoustic radiation force imaging: In vivo comparison to ultrasound motion tracking. Med. Phys. 2009; 36:2016–20. [PubMed: 19610290]

[215]. Arvanitis CD, McDannold N. Integrated ultrasound and magnetic resonance imaging for simultaneous temperature and cavitation monitoring during focused ultrasound therapies. Med. Phys. 2013; 34:1270–81.

[216]. Delso G, Furst S, Jakoby B, Ladebeck R, Ganter C, Nekolla SG, Schwaiger M, Ziegler SI. Performance measurements of the Siemens mMR integrated whole-body PET/MR scanner. J. Nucl. Med. 2011; 52:1914–22. [PubMed: 22080447]

[217]. ter Haar G, Sinnett D, Rivens I. High intensity focused ultrasound–a surgical technique for the treatment of discrete liver tumours. J. Nucl. Med. 1989; 34:1743–50.

[218]. Hynynen K, Freund WR, Cline HE, Chung AH, Watkins RD, Vetro JP, Jolesz FA. A clinical, noninvasive, MR imaging-monitored ultrasound surgery method. Radiographics. 1996; 16:185–95. [PubMed: 10946699]

[219]. Kohler MO, Mougenot C, Quesson B, Enholm J, Le Bail B, Laurent C, Moonen CTW, Enholm GJ. Volumetric HIFU ablation under 3D guidance of rapid MRI thermometry. Med. Phys. 2009; 36:3521–35. [PubMed: 19746786]

[220]. Fennessy FM, Tempany CM. An update on magnetic resonance guided focused ultrasound surgery (MRgFUS) of uterine fibroids. Curr. Radiol. Rep. 2013; 51:136–46.

[221]. Stewart EA. Uterine fibroids. N. Engl. J. Med. 2015; 372:1646–55. [PubMed: 25901428]

[222]. McDannold N, Tempany CM, Fennessy FM, So MJ, Rybicki FJ, Stewart EA, Jolesz FA, Hynynen K. Uterine leiomyomas: MR imaging-based thermometry and thermal dosimetry during focused ultrasound thermal ablation. Radiology. 2006; 240:263–72. [PubMed: 16793983]

[223]. Lenard ZM, McDannold NJ, Fennessy FM, Stewart EA, Jolesz FA, Hynynen K, Tempany CM. Uterine leiomyomas: MR imaging-guided focused ultrasound surgery–imaging predictors of success. Radiology. 2008; 249:187–194. [PubMed: 18695211]

[224]. Fennessy FM, et al. Uterine leiomyomas: MR imaging-guided focused ultrasound surgery–results of different treatment protocols. Radiology. 2007; 243:885–93. [PubMed: 17446521]

[225]. Stewart EA, Rabinovici J, Tempany CMC, Inbar Y, Regan L, Gastout B, Hesley G, Kim HS, Hengst S, Gedroye WM. Clinical outcomes of focused ultrasound surgery for the treatment of uterine fibroids. Fertil. Steril. 2006; 85:22–9. [PubMed: 16412721]

[226]. Al Hilli MM, Stewart EA. Magnetic resonance-guided focused ultrasound surgery. Semin. Reprod. Med. 2010; 28:242–9. [PubMed: 20414847]

[227]. Kim Y-S, Kim J-H, Rhim H, Lim HK, Keserci B, Bae D-S, Kim B-G, Lee J-W, Kim T-J, Choi CH. Volumetric MR-guided high-intensity focused ultrasound ablation with a one-layer strategy to treat large uterine fibroids: initial clinical outcomes. Radiology. 2012; 263:600–9. [PubMed: 22403170]

[228]. Ellens N, Hynynen K. Simulation study of the effects of near- and far-field heating during focused ultrasound uterine fibroid ablation using an electronically focused phased array: a theoretical analysis of patient safety. Med. Phys. 2014; 41:072902. 15pp. [PubMed: 24989412]

[229]. Falkmer U, Jarhult J, Wersall P, Cavallin-stahl E. A systematic overview of radiation therapy effects in skeletal metastases. Acta. Oncol. 2003; 42:620–33. [PubMed: 14596519]

[230]. Chow E, Hoskin P, van der Linden Y, Bottomley A, Velikova G. Quality of life and symptom end points in palliative bone metastases trials. Clin. Oncol. 2006; 18:67–9.

[231]. Smith NB, Temkin JM, Shapiro F, Hynynen K. Thermal effects of focused ultrasound energy on bone tissue. Ultrasound Med. Biol. 2001; 27:1427–33. [PubMed: 11731056]

[232]. Huisman M, Lam MK, Bartels LW, Nijenhuis RJ, Moonen CT, Knuttel FM, Verkooijen HM, van Vulpen M, van den Bosch MA. Feasibility of volumetric MRI-guided high intensity focused ultrasound (MR-HIFU) for painful bone metastases. J. Ther. Ultrasound. 2014; 216 10pp.

[233]. Hurwitz MD, et al. Magnetic resonance-guided focused ultrasound for patients with painful bone metastases: phase III trial results. J. Natl. Cancer Inst. 2014; 106 dju082 (9pp).

[234]. Weeks EM, Platt MW, Gedroyc W. MRI-guided focused ultrasound (MRgFUS) to treat facet joint osteoarthritis low back pain–case series of an innovative new technique. Eur. Radiol. 2012; 22:2822–35. [PubMed: 22935902]

[235]. Joo B, Park M-S, Lee SH, Choi HJ, Lim ST, Rha SY, Rachmilevitch I, Lee YH, Suh J-S. Pain palliation in patients with bone metastases using magnetic resonance-guided focused ultrasound with conformal bone system: a preliminary report. Yonsei Med. J. 2015; 56:503–9. [PubMed: 25684002]

[236]. Siegel RL, Miller KD, Jernal A. Cancer statistics, 2015. CA. Cancer J. Clin. 2015; 65:5–29. [PubMed: 25559415]

[237]. Potosky AL, Davis WW, Hoffman RM, Stanford JL, Stephensen RA, Penson DF, Harlan LC. Five-year outcomes after prostatectomy or radiotherapy for prostate cancer: the prostate cancer outcomes study. J. Natl. Cancer Inst. 2004; 96:1358–67. [PubMed: 15367568]

[238]. Crouzet S, Chapelon JY, Rouviere O, Mege-Lechevallier F, Colombel M, Tonoli-Catez H, Martin X, Gelet A. Whole-gland ablation of localized prostate cancer with high-intensity focused ultrasound: oncologic outcomes and morbidity in 1002 patients. Eur. Urol. 2014; 65:907–14. [PubMed: 23669165]

[239]. Napoli A, Anzidei M, De Nunzio C, Cartocci G, Panebianco V, De Dominicis C, Catalano C, Petrucci F, Leonardo C. Real-time magnetic resonance-guided high-intensity focused ultrasound focal therapy for localised prostate cancer: preliminary experience. Eur. Urol. 2013; 63:395–8. [PubMed: 23159454]

[240]. Fry FJ, Barger JE. Acoustical properties of the human skull. J. Acoust. Soc. Am. 1978; 63:1576–90. [PubMed: 690336]

[241]. Connor CW, Hynynen K. Patterns of thermal deposition in the skull during transcranial focused ultrasound surgery. IEEE Trans. Biomed. Eng. 2004; 51:1693–706. [PubMed: 15490817]

[242]. Pinton G, Aubry JF, Bossy E, Muller M, Pernot M, Tanter M. Attenuation, scattering, and absorption of ultrasound in the skull bone. Med. Phys. 2012; 39:299–307. [PubMed: 22225300]

[243]. Fry FJ, Goss SA. Further studies of the transkull transmission of an intense focused ultrasonic beam: lesion production at 500 kHz. Ultrasound Med. Biol. 1980; 6:33–8. [PubMed: 7368418]

[244]. Sun J, Hynynen K. Focusing of therapeutic ultrasound through a human skull: a numerical study. J. Acoust. Soc. Am. 1998; 104:1705–15. [PubMed: 9745750]

[245]. Sun J, Hynynen K. The potential of transskull ultrasound therapy and surgery using the maximum available skull surface area. J. Acoust. Soc. Am. 1999; 105:2519–27. [PubMed: 10212433]

[246]. Clement GT, Sun J, Giesecke T, Hynynen K. A hemisphere array for non-invasive ultrasound brain therapy and surgery. Phys. Med. Biol. 2000; 45:3707–19. [PubMed: 11131194]

[247]. Clement GT, White J, Hynynen K. Investigation of a large-area phased array for focused ultrasound surgery through the skull. Phys. Med. Biol. 2000; 45:1071–83. [PubMed: 10795992]

[248]. McDannold NJ, Vykhodtseva NI, Hynynen K. Microbubble contrast agent with focused ultrasound to create brain lesions at low power levels: MR imaging and histologic study in rabbits. Radiology. 2006; 241:95–106. [PubMed: 16990673]

[249]. Connor CW, Clement GT, Hynynen K. A unified model for the speed of sound in cranial bone based on genetic algorithm optimization. Phys. Med. Biol. 2002; 47:3925–44. [PubMed: 12476974]

[250]. Pichardo S, Sin VW, Hynynen K. Multi-frequency characterization of the speed of sound and attenuation coefficient for longitudinal transmission of freshly excised human skulls. Phys. Med. Biol. 2011; 56:219–50. [PubMed: 21149950]

[251]. Hynynen K, Clement GT, McDannold N, Vykhodtseva N, King R, White PJ, Vitek S, Jolesz FA. 500-Element Ultrasound Phased Array System for Noninvasive Focal Surgery of the Brain: A

Preliminary Rabbit Study With Ex Vivo Human Skull. Magn. Reson. Med. 2004; 52:100–7. [PubMed: 15236372]

[252]. McDannold N, King RL, Hynynen K. MRI monitoring of heating produced by ultrasound absorption in the skull: in vivo study in pigs. Magn. Reson. Med. 2004; 51:1061–5. [PubMed: 15122691]

[253]. Hynynen K, McDannold N, Clement G, Jolesz FA, Zadicario E, Killiany R, Moore T, Rosen D. Pre-clinical testing of a phased array ultrasound system for MRI-guided noninvasive surgery of the brain–a primate study. Eur. J. Radiol. 2006; 59:149–56. [PubMed: 16716552]

[254]. Elias WJ, et al. A pilot study of focused ultrasound thalamotomy for essential tremor. N. Engl. J. Med. 2013; 369:640–8. [PubMed: 23944301]

[255]. Lipsman N, Shwartz ML, Huang Y, Liesly L, Sankar T, Chapman M, Hynynen K, Lozano AM. MR-guided focused ultrasound thalamotomy for essential tremor: a proof-of-concept study. Lancet Neurol. 2013; 12:462–8. [PubMed: 23523144]

[256]. Chang WS, Jung HH, Kweon EJ, Zadicario E, Rachmilevitch I, Chang JW. Unilateral magnetic resonance guided focused ultrasound thalamotomy for essential tremor: practices and clinicoradiological outcomes. J. Neurol. Neurosurg. Psychiatry. 2014; 86:257–64. [PubMed: 24876191]

[257]. Ram Z, Cohen ZR, Harnof S, Tal S, Faibel M, Nass D, Maier SE, Hadani M, Yael Mardor. Magnetic resonance imaging-guided, high-intensity focused ultrasound for brain tumor therapy. Neurosurgery. 2006; 59:949–55. [PubMed: 17143231]

[258]. Coluccia D, Fandino J, Schwyzer L, O'Gorman R, Remonda L, Anon J, Martin E, Werner B. First noninvasive thermal ablation of a brain tumor with MR-guided focused ultrasound. J. Ther. Ultrasound. 2014; 2:17. 7pp. [PubMed: 25671132]

[259]. Martin E, Jeanmonod D, Morel A, Zadicario E, Werner B. High-intensity focused ultrasound for noninvasive functional neurosurgery. Ann. Neurol. 2009; 66:858–61. [PubMed: 20033983]

[260]. Jung HH, Kim SJ, Chang JG, Chang WS, Kweon EJ, Kim C-H, Chang JW. Bilateral thermal capsulotomy with MR-guided focused ultrasound for patients with treatment-refractory obsessive-compulsive disorder: a proof-of-concept study. Mol. Psychiatry. 2014; 20:1205–11. [PubMed: 25421403]

[261]. Magara A, Buhler R, Moser D, Kowalski M, Pourtehrani P, Jeanmonod D. First experience with MR-guided focused ultrasound in the treatment of Parkinson's disease. J. Ther. Ultrasound. 2014; 2:11. 8pp. [PubMed: 25512869]

[262]. Lipsman N, Mainprize TG, Schwartz ML, Hynynen K, Lozano AM. Intracranial Applications of Magnetic Resonance-guided Focused Ultrasound. Neurotherapeutics. 2014; 11:593–605. [PubMed: 24850310]

[263]. Gianfelice D, Khiat A, Amara M, Belblidia A, Boulanger Y. MR imaging-guided focused ultrasound surgery of breast cancer: correlation of dynamic contrast-enhanced MRI with histopathologic findings. Breast Cancer Res. Treat. 2003; 82:93–101. [PubMed: 14692653]

[264]. Okada A, Murakami T, Mikami K, Onishi H, Tanigawa N, Marukawa T, Nakamura H. A case of hepatocellular carcinoma treated by MR-guided focused ultrasound ablation with respiratory gating. Magn. Reson. Med. Sci. 2006; 5:167–71. [PubMed: 17139143]

[265]. Gedroyc WM. New clinical applications of magnetic resonance-guided focused ultrasound. Top. Magn. Reson. Imaging. 2006; 17:189–94. [PubMed: 17414076]

[266]. ter Haar GR. High intensity focused ultrasound for the treatment of tumors. Echocardiography. 2001; 18:317–22. [PubMed: 11415504]

[267]. Payne A, et al. Design and characterization of a laterally mounted phased-array transducer breast-specific MRgHIFU device with integrated 11-channel receiver array. Med. Phys. 2012; 39:1552–60. [PubMed: 22380387]

[268]. Merckel LG, Bartels LW, Kohler MO, Desiree van den Bongard HJG, Deckers R, Mali WPTM, Binkert CA, Moonen CT, Gilhuijs KGA, van den Bosch MAAJ. MR-guided high-intensity focused ultrasound ablation of breast cancer with a dedicated breast platform. Cardiovasc. Intervent. Radiol. 2013; 36:292–301. [PubMed: 23232856]

[269]. de Senneville BD, Mougenot C, Moonen CTW. Real-time adaptive methods for treatment of mobile organs by MRI-controlled high-intensity focused ultrasound. Magn. Reson. Med. 2007; 57:319–30. [PubMed: 17260361]

[270]. Tanter M, Pernot M, Aubry J-F, Montaldo G, Marquet F, Fink M. Compensating for bone interfaces and respiratory motion in high-intensity focused ultrasound. Int. J. Hyperthermia. 2007; 23:141–51. [PubMed: 17578338]

[271]. Daum DR, Smith NB, King R, Hynynen K. *In vivo* demonstration of noninvasive thermal surgery of the liver and kidney using an ultrasonic phased array. Ultrasound Med. Biol. 1999; 25:1087–98. [PubMed: 10574341]

[272]. Civale J, Clarke R, Rivens I, ter Haar G. The use of a segmented transducer for rib sparing in HIFU treatments. Ultrasound Med. Biol. 2006; 32:1753–61. [PubMed: 17112961]

[273]. Staruch RM, Ganguly M, Tannock IF, Hynynen K, Chopra R. Enhanced drug delivery in rabbit VX2 tumours using thermosensitive liposomes and MRI-controlled focused ultrasound hyperthermia. Int. J. Hyperthermia. 2012; 28:776–87. [PubMed: 23153219]

[274]. Partanen, et al. Mild hyperthermia with magnetic resonance-guided high-intensity focused ultrasound for applications in drug delivery. Int. J. Hyperthermia. 2012; 28:320–36. [PubMed: 22621734]

[275]. Staruch RM, Hynynen K, Chopra R. Hyperthermia-mediated doxorubicin release from thermosensitive liposomes using MR-HIFU: Therapeutic effect in rabbit Vx2 tumours. Int. J. Hyperthermia. 2015; 31:118–33. [PubMed: 25582131]

[276]. McDannold N, Arvanitis CD, Vykhodtseva N, Livingstone MS. Temporary disruption of the blood-brain barrier by use of ultrasound and microbubbles: safety and efficacy evaluation in rhesus macaques. Cancer Res. 2012; 72:3652–63. [PubMed: 22552291]

[277]. Monteith SJ, et al. Minimally invasive treatment of intracerebral hemorrhage with magnetic resonance-guided focused ultrasound. J. Neurosurg. 2013; 118:1035–45. [PubMed: 23330996]

[278]. Arvanitis CD, Vykhodtseva, Jolesz F, Livingstone M, McDannold N. Cavitation-enhanced nonthermal ablation in deep brain targets: feasibility in a large animal model. J. Neurosurg. 2015 E-pub ahead of print.

[279]. Xu Z, et al. Intracranial inertial cavitation threshold and thermal ablation lesion creation using MRI-guided 220-kHz focused ultrasound surgery: preclinical investigation. J. Neurosurg. 2014; 122:152–61. [PubMed: 25380106]

[280]. Alkins R, Huang Y, Pajek D, Hynynen K. Cavitation-based third ventriculostomy using MRI-guided focused ultrasound. J. Neurosurg. 2013; 119:1520–9. [PubMed: 24074494]

[281]. Marquet F, Boch A-L, Pernot M, Montaldo G, Seilhean D, Fink M, Tanter M, Aubry J-F. Non-invasive ultrasonic surgery of the brain in non-human primates. J. Acoust. Soc. Am. 2013; 134:1632–9. [PubMed: 23927203]

[282]. Aubry J-F, et al. Ultrasons focalises de forte intensite pour la therapie transcranienne du cerveau. IRBM. 2010; 31:87–91.

[283]. Chauvet D, et al. Targeting accuracy of transcranial magnetic resonance-guided high-intensity focused ultrasound brain therapy: a fresh cadaver model. J. Neurosurg. 2013; 118:1046–52. [PubMed: 23451909]

[284]. Liu H-L, et al. Design and experimental evaluation of a 256-channel dual-frequency ultrasound phased-array system for transcranial blood-brain barrier opening and brain drug delivery. IEEE Trans. Biomed. Eng. 2014; 61:1350–60. [PubMed: 24658258]

[285]. Kim Y, Hall TL, Xu Z, Cain CA. Transcranial histotripsy therapy: a feasibility study. IEEE Trans. Ultrason. Ferroelectr. Freq. Control. 2014; 61:582–93.

[286]. Zimmer JE, Hynynen K, He DS, Marcus F. The feasibility of using ultrasound for cardiac ablation. IEEE Trans. Biomed. Eng. 1995; 42:891–7. [PubMed: 7558063]

[287]. Hynynen K, Dennie J, Zimmer JE, Simmons WN, He DS, Marcus FI, Aguirre M. Cylindrical ultrasonic transducers for cardiac catheter ablation. IEEE Trans. Ultrason. Ferroelectr. Freq. Control. 1997; 44:144–151.

[288]. Stephens DN, et al. First in vivo use of a capacitive micromachined ultrasound transducer array-based imaging and ablation catheter. J. Ultrasound Med. 2012; 31:247–56. [PubMed: 22298868]

[289]. Pichardo S, Hynynen K. New design for an endoesophageal sector-based array for the treatment of atrial fibrillation: a parametric simulation study. IEEE Trans. Ultrason. Ferroelectr. Freq. Control. 2009; 56:600–11. [PubMed: 19411218]

[290]. Werner J, Park E-J, Lee H, Francischelli D, Smith NB. Feasibility of in vivo transesophageal cardiac ablation using a phased ultrasound array. Ultrasound Med. Biol. 2010; 36:752–60. [PubMed: 20347517]

[291]. Constanciel E, D'Jin WA, Bessiere F, Chavrier F, Grinberg D, Vignot A, Chevalier P, Chapelon JY, Lafon C. Design and evaluation of a transesophageal HIFU probe for ultrasound-guided cardiac ablation: simulation of a HIFU mini-maze procedure and preliminary ex vivo trials. IEEE Trans. Ultrason. Ferroelectr. Freq. Control. 2013; 60:1868–83. [PubMed: 24658718]

[292]. Gross D, Coutier C, Legros M, Bouakaz A, Certon D. A cMUT probe for ultrasound-guided focused ultrasound targeted therapy. IEEE Trans. Ultrason. Ferroelectr. Freq. Control. 2015; 62:1145–60. [PubMed: 26067049]

[293]. Almekkaway MK, Shehata IA, Ebbini ES. Anatomical-based model for simulation of HIFU-induced lesions in atherosclerotic plaques. Int. J. Hyperthermia. 2015; 31:433–42. [PubMed: 25875223]

[294]. Goertz DE. An overview of the influence of therapeutic ultrasound exposures on the vasculature: high intensity ultrasound and microbubble-mediated bioeffects. Int. J. Hyperthermia. 2015; 31:134–44. [PubMed: 25716770]

[295]. Delon-Martin C, Vogt C, Chignier E, Guers C, Chapelon JY, Cathignol D. Venous thrombosis generation by means of high-intensity focused ultrasound. Ultrasound Med. Biol. 1995; 21:113–9. [PubMed: 7754571]

[296]. Hynynen K, Colucci V, Chung A, Jolesz F. Noninvasive arterial occlusion using MRI-guided focused ultrasound. Ultrasound Med. Biol. 1996; 22:1071–7. [PubMed: 9004431]

[297]. Vaezy S, Martin R, Yaziji H, Kaczkowski P, Keilman G, Carter S, Caps M, Chi YM, Bailey M, Crum L. Hemostasis of punctured blood vessels using high-intensity focused ultrasound. Ultrasound Med. Biol.l. 1998; 24:903–10.

[298]. Vaezy S, et al. Control of splenic bleeding by using high intensity ultrasound. J. Trauma. 1999; 47:521–5. [PubMed: 10498307]

[299]. Zderic V, O'Keefe GE, Foley JL, Vaezy S. Resection of abdominal solid organs using high-intensity focused ultrasound. Ultrasound Med. Biol. 2007; 33:1251–8. [PubMed: 17498864]

[300]. Oosterhof GON, Cornel EB, Smits GAHJ, Debruyne FMJ, Schalken JA. The influence of high-energy shock waves on the development of metastases. Ultrasound Med. Biol. 1996; 22:339–44. [PubMed: 8783466]

[301]. Miller DL, Dou C, Song J. Lithotripter shockwave-induced enhancement of mouse melanoma lung metastasis: dependence on cavitation nucleation. J. Endourol. 2004; 18:925–9. [PubMed: 15659934]

[302]. Miller DL, Dou C. The potential for enhancement of mouse melanoma metastasis by diagnostic and high-amplitude ultrasound. Ultrasound Med. Biol. 2006; 32:1097–1101. [PubMed: 16829323]

[303]. Hu Z, Yang XY, Liu Y, Sankin GN, Pua EC, Morse MA, Lyerly HK, Clay TM, Zhong P. Investigation of HIFU-induced anti-tumor immunity in a murine tumor model. J. Transl. Med. 2007; 5:34. 11pp. [PubMed: 17625013]

[304]. Xing Y, Lu X, Pua EC, Zhong P. The effect of high intensity focused ultrasound treatment on metastases in a murine melanoma model. Biochem. Biophys. Res. Commun. 2008; 375:645–50. [PubMed: 18727919]

[305]. Konofagou EE. Optimization of the ultrasound-induced blood-brain barrier opening. Theranostics. 2012; 2:1223–37. [PubMed: 23382778]

[306]. Aryal M, Arvanitis CD, Alexander PM, McDannold N. Ultrasound-mediated blood-brain barrier disruption for targeted drug delivery in the central nervous system. Adv. Drug Deliv. Rev. 2014; 72:94–109. [PubMed: 24462453]

[307]. Burgess A, Hynynen K. Drug delivery across the blood-brain barrier using focused ultrasound. Expert Opin. Drug Deliv. 2014; 11:5. 11pp. [PubMed: 24073618]

[308]. Liu H-L, Hua M-Y, Chen P-Y, Chu P-C, Pan C-H, Yang H-W, Huang C-Y, Wang J-J, Yen T-C, Wei K-C. Blood-brain barrier disruption with focused ultrasound enhances delivery of chemotherapeutic drugs for glioblastoma treatment. Radiology. 2010; 255:415–25. [PubMed: 20413754]

[309]. Treat LH, McDannold N, Zhang Y, Vykhodtseva N, Hynynen K. Improved anti-tumor effect of liposomal doxorubicin after targeted blood-brain barrier disruption by MRI-guided focused ultrasound in rat glioma. Ultrasound Med. Biol. 2012; 38:1716–25. [PubMed: 22818878]

[310]. Aryal M, Vykhodtseva N, Zhang Y-Z, Park J, McDannold N. Multiple treatments with liposomal doxorubicin and ultrasound-induced disruption of blood-tumor and blood-brain barriers improve outcomes in a rat glioma model. J. Control. Release. 2013; 169:103–11. [PubMed: 23603615]

[311]. Burgess A, Dubey S, Yeng S, Hough O, Eterman N, Aubert I, Hynynen K. Alzheimer disease in a mouse model: MR imaging-guided focused ultrasound targeted to the hippocampus opens the blood-brain barrier and improves pathologic abnormalities and behavior. Radiology. 2014; 237:736–45. [PubMed: 25222068]

[312]. Leinenga G, Gotz J. Scanning ultrasound removes amyloid-β and restores memory in an Alzheimer's disease mouse model. Sci. Transl. Med. 2014; 7:278ra33. 11pp.

[313]. Samiotaki G, Acosta C, Wang S, Konofagou EE. Enhanced delivery and bioactivity of the neurturin neurotrophic factor through focused ultrasound-mediated blood–brain barrier opening in vivo. J. Cereb. Blood Flow Metab. 2015; 35:611–22. [PubMed: 25586140]

[314]. Burgess A, Huang Y, Waspe AC, Ganguly M, Goertz DE, Hynynen K. High-intensity focused ultrasound (HIFU) for dissolution of clots in a rabbit model of embolic stroke. Public Libr. Sci. One. 2012; 7:e42311. 7pp.

[315]. Maxwell AD, Owens G, Gurm HS, Ives K, Myers DD, Xu Z. Noninvasive treatment of deep venous thrombosis using pulsed ultrasound cavitation therapy (histotripsy) in a porcine model. J. Vasc. Interv. Radiol. 2011; 22:369–77. [PubMed: 21194969]

[316]. Rosenschein U, Furman V, Kerner E, Fabian I, Bernheim J, Eshel Y. Ultrasound imaging-guided noninvasive ultrasound thrombolysis: preclinical results. Circulation. 2000; 102:238–45. [PubMed: 10889137]

[317]. Harnof S, Zibly Z, Hananel A, Monteith S, Grinfield J, Schiff G, Kulbatski I, Kassell N. Potential of magnetic resonance-guided focused ultrasound for intracranial hemorrhage: an *in vivo* feasibility study. J. Stroke Cerebrovasc. Des. 2014; 23:1585–91.

[318]. Alexandrov, et al. Ultrasound-enhanced thrombolysis for acute ischemic stroke. N. Engl. J. Med. 2004; 14:113–7.

[319]. Petit E, Bohren Y, Gaud E, Bussat P, Arditi M, Yan F, Tranquart F, Allemann E. Sonothrombolysis: the contribution of stable and inertial cavitation to clot lysis. Ultrasound Med. Biol. 2015; 41:1402–10. [PubMed: 25601463]

[320]. Brown AT, Flores R, Hamilton E, Roberson PK, Morrelli MJ, Culp WC. Microbubbles improve sonothrombolysis in vitro and decrease hemorrhage in vivo in a rabbit stroke model. Invest. Radiol. 2011; 46:202–7. [PubMed: 21150788]

[321]. Molina CA, et al. Microbubble administration accelerates clot lysis during continuous 2-MHz ultrasound monitoring in stroke patients treated with intravenous tissue plasminogen activator. Stroke. 2006; 37:425–9. [PubMed: 16373632]

[322]. Braak E, Braak H. Neuropathological stageing of Alzheimer-related changes. Acta. Neuropathol. 1991; 82:239–59. [PubMed: 1759558]

[323]. Braak H, Del Tredici K, Rub U, de Vos RAI, Steur ENHJ, Braak E. Staging of brain pathology related to sporadic Parkinson's disease. Neurobiol. Aging. 2003; 24:197–211. [PubMed: 12498954]

[324]. Yamamoto Y, Georgiadis AL, Chang H-M, Caplan LR. Posterior cerebral artery territory infarcts in the New England Medical Center Posterior Circulation Registry. Arch. Neurol. 1999; 56:824–32. [PubMed: 10404984]

[325]. Bogousslavsky J, Regli F. Anterior cerebral artery territory infarction in the Lausanne Stroke Registry: clinical and etiologic patterns. Arch. Neurol. 1990; 47:144–50. [PubMed: 2302085]

[326]. Wood AKW, Sehgal CM. A review of low-intensity ultrasound for cancer therapy. Ultrasound Med. Biol. 2015; 41:905–28. [PubMed: 25728459]

[327]. Guilhon E, et al. Spatial and temporal control of transgene expression in vivo using a heat-sensitive promoter and MRI-guided focused ultrasound. J. Gene Med. 2003; 5:333–42. [PubMed: 12692867]

[328]. Silcox CE, Smith RC, King R, McDannold N, Bromley P, Walsh K, Hynynen K. MRI-guided ultrasonic heating allows spatial control of exogenous luciferase in canine prostate. Ultrasound Med. Biol. 2005; 31:965–70. [PubMed: 15972202]

[329]. Unger EC, Porter T, Culp W, Labell R, Matsunaga T, Zutshi R. Therapeutic applications of lipid-coated microbubbles. Adv. Drug Deliv. Rev. 2004; 56:1291–1314. [PubMed: 15109770]

[330]. Hernot S, Klibanov AL. Microbubbles in ultrasound-triggered drug and gene delivery. Adv. Drug Deliv. Rev. 2008; 60:1153–66. [PubMed: 18486268]

[331]. Bekeredjian R, Chen S, Frenkel PA, Grayburn PA, Shohet RV. Ultrasound-targeted microbubble destruction can repeatedly direct highly specific plasmid expression to the heart. Circulation. 2003; 108:1022–6. [PubMed: 12912823]

[332]. Brayman AA, Lizotte LM, Miller MW. Erosion of artificial endothelia in vitro by pulsed ultrasound: acoustic pressure, frequency, membrane orientation and microbubble contrast agent dependence. Ultrasound Med. Biol. 1999; 25:1305–20. [PubMed: 10576273]

[333]. Greenleaf WJ, Bolaner ME, Sarkar G, Goldring MB, Greenleaf JM. Artificial cavitation nuclei significantly enhance acoustically induced cell transfection. Ultrasound Med. Biol. 1998; 24:587–95. [PubMed: 9651968]

[334]. Dougherty TJ, Gomer CJ, Henderson BW, Jori G, Kessel D, Korbelik M, Moan J, Peng Q. Photodynamic therapy. J. Natl. Cancer Inst. 1998; 90:889–905. [PubMed: 9637138]

[335]. Umemura S, Yumita N, Nishigaki R, Umemura K. Sonochemical activation of hematoporphyrin: a potential modality for cancer treatment. Proc. IEEE Ultrason. Symp. 1989:955–60.

[336]. Costley D, Mc Ewan C, Fowley C, McHale AP, Atchison J, Nomikou N, Callan JF. Treating cancer with sonodynamic therapy: a review. Int. J. Hyperthermia. 2015; 31:107–17. [PubMed: 25582025]

[337]. Colucci V, Strichartz G, Jolesz F, Vykhodtseva N, Hynynen K. Focused ultrasound effects on nerve action potential. in vitro Ultrasound Med. Biol. 2009; 35:1737–47. [PubMed: 19647923]

[338]. Foley JL, Little JW, Vaezy S. Effects of high-intensity focused ultrasound on nerve conduction. Muscle Nerve. 2008; 37:241–50. [PubMed: 18041054]

[339]. Foley JL, Little JW, Staar FL, Frantz C, Vaezy S. Image-guided HIFU neurolysis of peripheral nerves to treat spasticity and pain. Ultrasound Med. Biol. 2004; 30:1199–1207. [PubMed: 15550323]

[340]. Gavrilov LR, Tsirulnikov EM, Davies II. Application of focused ultrasound for the stimulation of neural structures. Ultrasound Med. Biol. 1996; 22:179–92. [PubMed: 8735528]

[341]. Legon W, Sato TF, Opitz A, Mueller J, Barbour A, Williams A, Tyler WJ. Transcranial focused ultrasound modulates the activity of primary somatosensory cortex in humans. Nat. Neurosci. 2014; 17:322–9. [PubMed: 24413698]

[342]. Mueller J, Legon W, Opitz A, Sato TF, Tyler WJ. Transcranial focused ultrasound modulates intrinsic and evoked EEG dynamics. Brain Stimul. 2014; 7:900–8. [PubMed: 25265863]

[343]. Menz MD, Oralkan O, Khuri-Yakub P, Baccus SA. Precise neural stimulation in the retina using focused ultrasound. J. Neurosci. 2013; 33:4550–60. [PubMed: 23467371]

[344]. Moreno-Moraga J, Valero-Altes T, Riquelme AM, Isarria-Marcosy MI, de la Torre JR. Body contouring by non-invasive transdermal focused ultrasound. Lasers Surg. Med. 2007; 39:315–23. [PubMed: 17457840]

[345]. Jewell ML, et al. Safety and tolerability of high-intensity focused ultrasonography for noninvasive body sculpting: 24-week data from a randomized, sham-controlled study. Aesthet. Surg. J. 2012; 32:868–76. [PubMed: 22942114]

[346]. MacGregor JL, Tanzi EL. Microfocused ultrasound for skin tightening. Semin. Cutan. Med. Surg. 2013; 32:18–25. [PubMed: 24049925]

[347]. Minkis K, Alam M. Ultrasound skin tightening. Dermatol. Clin. 2014; 32:71–7. [PubMed: 24267423]

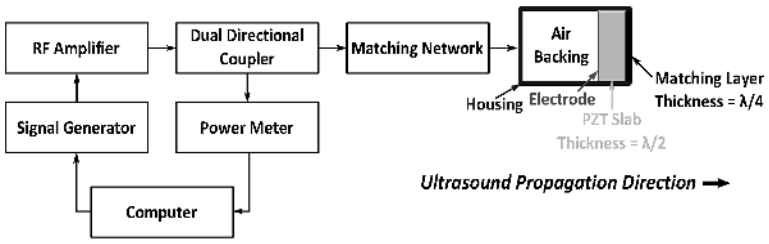


**Figure 1.**

Diagram of a single-element therapy transducer and its accompanying RF-driving line. For multi-element phased arrays, this driving line is repeated for each individual element.

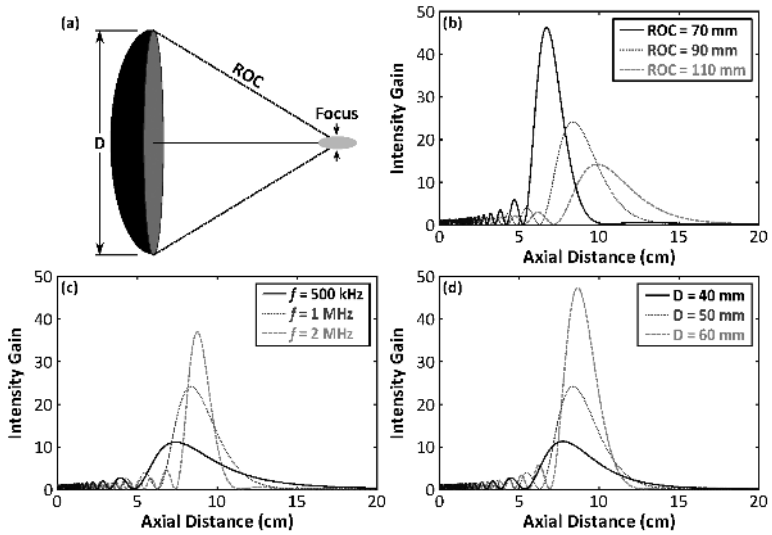


**Figure 2.**

Axial intensity plots for various spherically-focused, single-element transducers. (a) Transducer diagram. The effects of varying the (b) radius of curvature (ROC; $f$ = 1 MHz, D = 50 mm), frequency ($f$; ROC = 90 mm, D = 50 mm), and diameter (D; $f$ = 1 MHz, ROC = 90 mm) were simulated for conditions of linear ultrasound propagation in water.

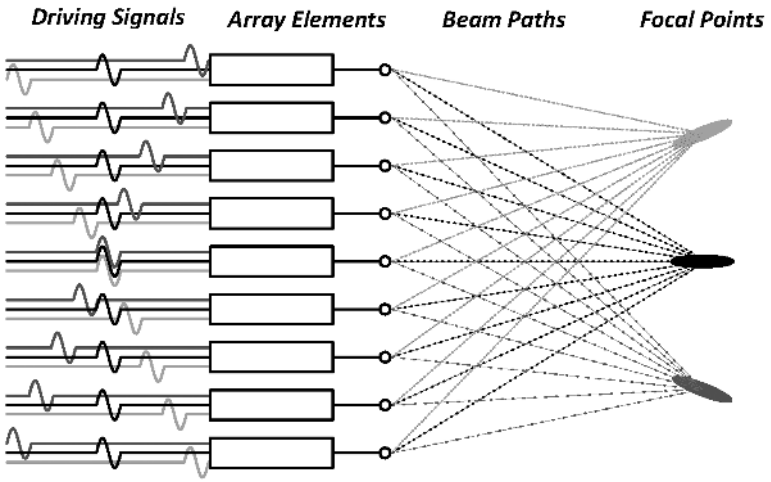


**Figure 3.**

Diagram demonstrating electronic beam steering on transmit with a lD linear array by adjusting the time at which individual elements are excited.

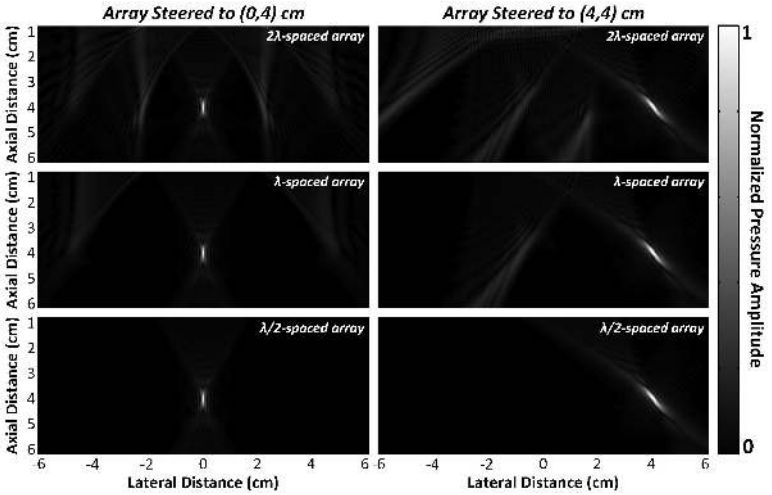


**Figure 4.**

Normalized axial pressure fields are plotted for 2D arrays (5 cm × 5 cm) with (top row) 32 × 32 2λ-spaced, (middle row) 64 × 64 λ-spaced, and (bottom row) 128 × 128 λ/2-spaced point source elements (2 MHz). Simulation results are shown for the case of electronic focusing to (0,4) cm (left column) and (4,4) cm (right column), for conditions of linear ultrasound propagation in water. Grating lobes are formed with the λ- and 2λ-spaced arrays, which become more prominent as the beam is steered away from the array's central axis.

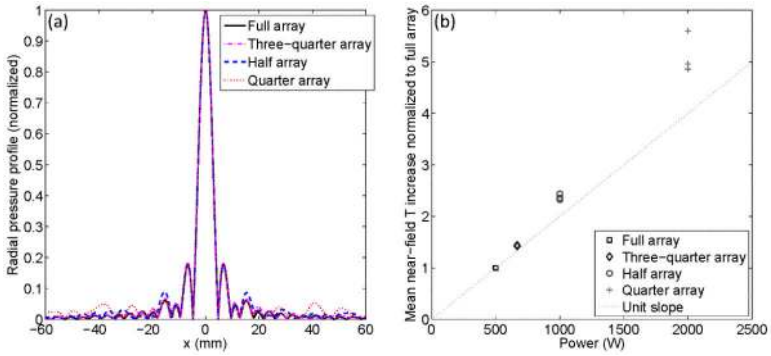


**Figure 5.**

Performance of flat, 2D random sparse arrays for FUS therapy [96]. (a) Lateral pressure profiles of random sparse arrays are shown with a different number of active elements relative to the full array (500 kHz, 4912 elements, element spacing = λ/2), which demonstrates good focal quality even with 253 of active elements. (b) Near-field temperature (T) elevation as a function of the acoustic power required to obtain the same focal temperature for each of the arrays, demonstrating that both the near-field heating and required power increase with increasing array sparsity.

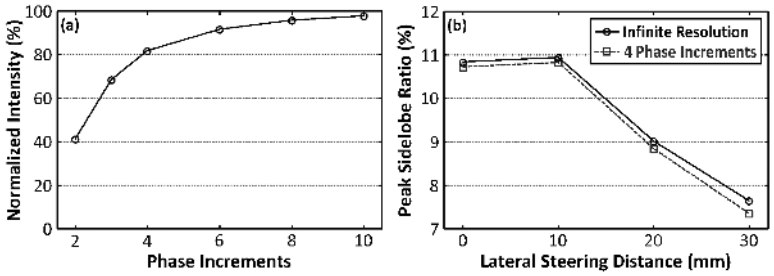


**Figure 6.**

(a) Peak focal intensity as a function of the number of phase increments, normalized to the case of infinite phase resolution. (b) Impact of phase resolution on the intensity peak sidelobe ratio. Simulated data for a fiat, 2D array (1.1 MHz, 128 × 128 elements, element spacing < λ/2) focused to (0,0,30) mm. The plots were re-drawn based on the data reported in the original article [104].

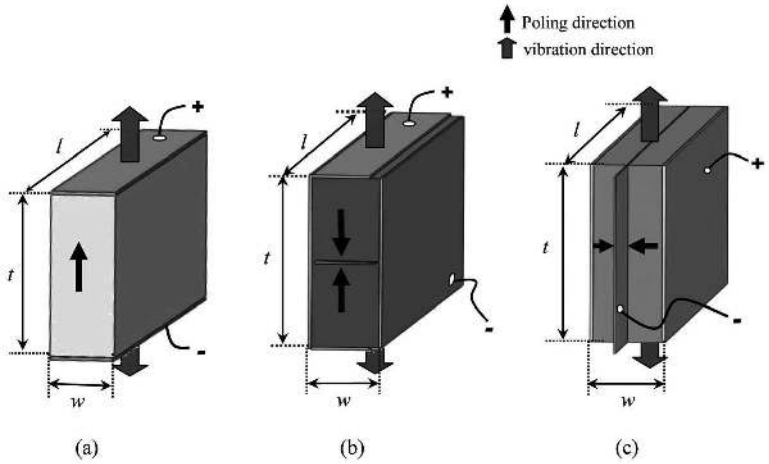


**Figure 7.**

Diagram of PZT elements driven in thickness mode and lateral coupling mode [108]. (a) A single layer PZT element driven in thickness mode. (b) A two-layer PZT element driven in thickness mode. (c) A two-layer lateral mode PZT element. The overall dimensions ($t$ = thickness, $l$ = length, $w$ = width) are the same for all three PZT elements.

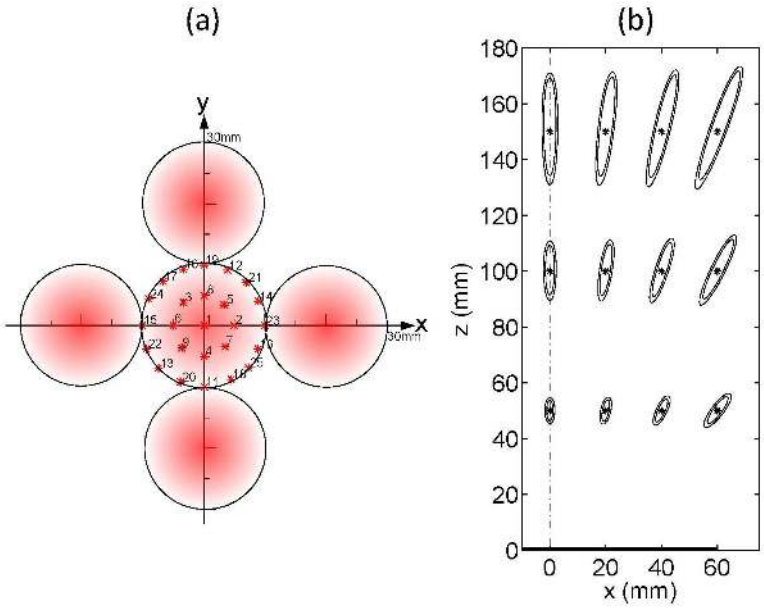


**Figure 8.**

(a) Example of a sonication raster pattern used to generate extended lesions [96]. Each of the five sonication cells contain 25 foci, shown in detail in the middle cell. (b) Simulated lesion projections (axial plane) for a fiat, 2D array (500 kHz, 4912 elements, element spacing = λ/2) with maximal temperatures of 60°C using a single sonication cell. The inner and outer contours correspond to 5 s and 20 s sonications, respectively [96].

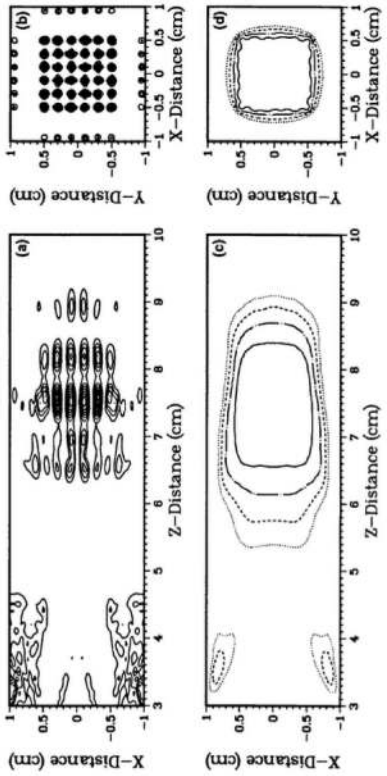


**Figure 9.**

Demonstration of multi-focus sonications using a phased array transducer [21]. The acoustic intensity deposition pattern (a,b) and lesion boundaries (c,d) obtained with a spherically-curved, 2D array (1.5 MHz, 256 elements). In (c,d), the maximum temperature level was 100°C (dotted line), 90°C (dashed line), 80°C (chained line), and 70°C (solid line). Plots (a,c) are axial planes (y = 0), while (b,d) are lateral planes (z = 7.9 cm).

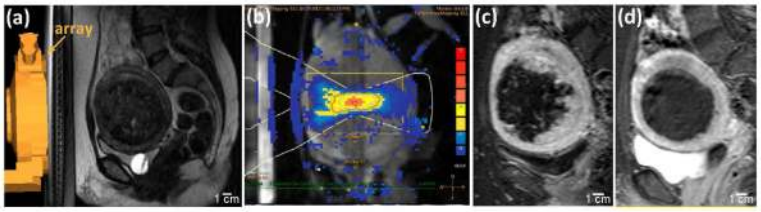


**Figure 10.**

Overview of MR-guided FUS therapy for uterine fibroids. (a) Pre-treatment, axial $T_2$-weighted MR image with a schematic of the array (Philips system) overlaid in orange. (b) Axial MRI-derived temperature map obtained during treatment. Axial contrast-enhanced $T_1$-weighted images taken (c) immediately and (d) 3 months after the treatment.

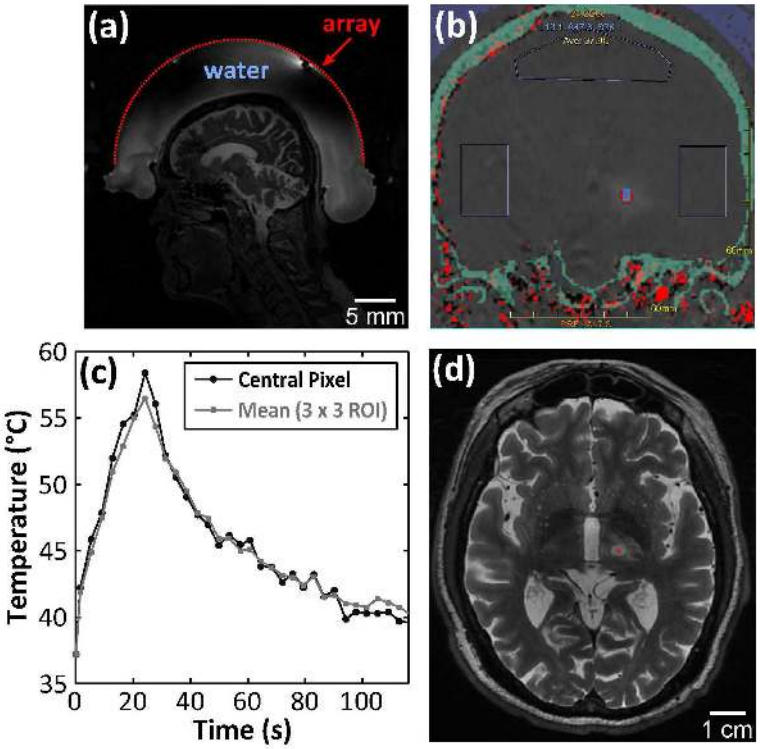


**Figure 11.**

Overview of MR-guided FUS therapy for essential tremor. (a) Pre-treatment sagittal MR image shows the orientation of the patient relative to the hemispherical transducer array, along with the circulating water for acoustic coupling and skull cooling. (b) Coronal MRI-derived temperature map obtained during treatment, with the patient's skull overlaid in green. (c) MRI-derived temperature profile near the focus during therapy, with curves for the mean temperature within a 3×3 pixel region of interest (ROI), along with the central pixel value. (d) Axial $T_2$-weighted MR image of the same patient shows a lesion in the patient's left thalamus (denoted by red asterisk) 1 day post-treatment.

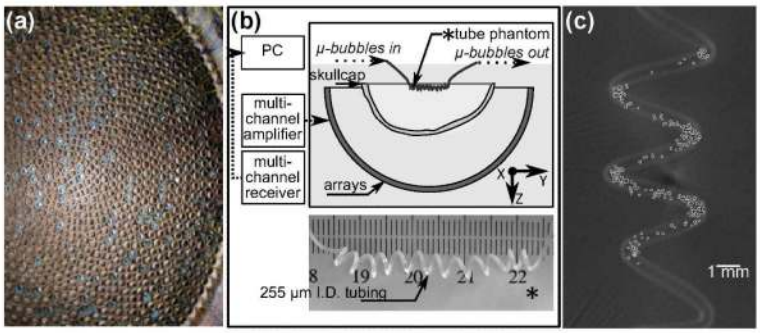


**Figure 12.**

An experimental transmit/receive array under development for trans-skull therapy and monitoring [137]. (a) Photo of the fully populated hemispherical transmit array with an optimized sparse receiver array. (b) Experimental setup for imaging microbubbles within a tube phantom through an *ex-vivo* human skullcap using the array. (c) Microbubble locations superimposed over a micro-CT of the tube phantom containing the bubbles.